

# **Development of the Passive Perfusion Probe for Non-invasive Blood Perfusion Measurement**

**Patricia Lynn Ricketts, B.S.**

Thesis submitted to the Faculty of the  
Virginia Polytechnic Institute and State University  
in partial fulfillment of the requirements for the degree of

**Master of Science**

in

**Mechanical Engineering**

Dr. Thomas E. Diller, Sc.D, Co-advisor

Dr. Elaine P. Scott, Ph.D., Co-advisor

Dr. Otto I. Lanz, DVM, Diplomate ACVS

May 3, 2007

Blacksburg, Virginia

Keywords: Blood Perfusion, Parameter Estimation, Phantom Tissue, Heat Flux

© Copyright by Patricia L. Ricketts, 2007

**Development of the Passive Perfusion Probe  
for Non-invasive Blood Perfusion Measurement**

Patricia L. Ricketts, B.S.

Virginia Polytechnic Institute and State University, 2007

Supervisor: Dr. Thomas E. Diller/Dr. Elaine P. Scott

**Abstract**

A non-invasive blood perfusion system has been developed and tested in a phantom tissue and an animal model. The system uses a small sensor with a laminated flat thermocouple to measure the heat transfer response to an arbitrary thermal event (convective or conductive) imposed on the tissue surface. Blood perfusion and contact resistance are estimated by comparing heat flux data with a mathematical model of the tissue. The perfusion system was evaluated for repeatability and sensitivity using both a phantom tissue test stand and exposed rat liver tests. Perfusion in the phantom tissue tests was varied by controlling the flow of water into the phantom tissue test section, and the perfusion in the exposed liver tests was varied by temporarily occluding blood flow through the portal vein. The phantom tissue tests indicated that the probe can be used to detect small changes in perfusion (0.009 ml/ml/s). The probe qualitatively tracked the changes in the perfusion of the liver model due to occlusion of the portal vein.

## **Attributions**

Dr. Diller has been my primary advisor for this research study. He envisioned the idea for the passive perfusion probe and implemented his design by manufacturing the probe. He was vital in the designing the pressed sensor technology and its manufacturing process. He assisted in establishing the experimental procedures for both the phantom tissue and rat liver models. Finally he assisted in selecting the data presented from the series of tests performed on both the non-living and living tissue models.

Dr. Scott has been the co-chair for my committee. She assisted in developing the finite difference model and parameter estimation routine used to estimate perfusion and contact resistance. She also assisted in the design of the phantom tissue test stand. She also assisted in selecting the data presented from the series of tests performed on both the non-living and living tissue models.

Dr. Lanz served as a member of my committee. He was essential in performing the living tissue tests as he conducted all testing on the rat livers. Also, he was instrumental in providing clinical insight to the project.

Ashvinikumar Mudaliar was a fellow lab mate of mine. He developed the finite difference model and parameter estimation code used to estimated perfusion and contact resistance for this work. Also, he developed the computational fluid dynamics model discussed and presented in this work. He also assisted in training me in the experimental procedures for both the non-living and living tissue tests.

Brent Ellis was also a fellow lab mate of mine. He began developing the pressed sensor technology in his research work and then passed the work on to me. He also assisted in designing the phantom tissue test stand and passive perfusion probe housing.

Clay Pullins was a student performing undergraduate research in my lab. He assisted in the design of the passive perfusion probe holder. He also assisted in conducting the testing on the non-living and living tissue models under my supervision.

Leah Meyers was also a student performing undergraduate research in my lab. She assisted in manufacturing the thin film thermocouples and laminated heat flux sensors. She also conducted testing on the non-living and living tissue models under my supervision.

## **Acknowledgments**

I would like to thank the members of my committee for their help and guidance throughout the duration of this project. I would like to thank Dr. Diller for giving me the opportunity to explore my interest in the field and especially for his great amount of sound advice during the project. I met Dr. Scott as a high school student and she first introduced me to this project when I was a sophomore at Virginia Tech. My involvement and understanding grew as a result of her encouragement and leadership through the years. I would like to thank her for being such a great advisor, mentor and role model. I would like to thank Dr. Lanz for his cooperation in conducting the animal tests at the veterinary school and for his clinical insight on the project.

I would also like to thank my fellow labmates, Ashvin, Brent, Clay and Leah, for helping me with this project and providing a fun work environment. I would also like to thank Barbara Kafka in the Small Animal Clinical Sciences Physiology Lab for all of her help in coordinating and conducting the animal tests at the veterinary school.

Next, I must thank my parents, Garland and Hazel, for their unwavering love and encouragement. Thanks for always supporting me, even when I had to do it *my* way. To the rest of my family, I am truly blessed to have you as both relatives and friends. Thanks for everything. I would like to thank Bruce for always knowing what I need, which is a good laugh most of the time.

To my friends, both near and far, and my person, thanks for making Virginia Tech the best home away from home anyone could ever ask for. Finally, I dedicate this work in remembrance of the lives lost during the tragic events of April 16, 2007. As long as life and memory last, we shall remember you.

Patricia L. Ricketts

*Virginia Polytechnic Institute and State University*  
*May 2007*

# Table of Contents

Thesis Abstract .....	i
Attributions .....	iii
Acknowledgments .....	v
Table of Contents .....	vi
List of Figures .....	viii
List of Tables .....	xi
Nomenclature .....	xii
Preface .....	xiii
Abstract .....	1
Introduction .....	2
Background on Perfusion Measuring Techniques .....	3
Pressed Sensor Technology .....	6
Perfusion Probe Design .....	6
Convective Laminated Perfusion Probe .....	7
Passive Perfusion Probe .....	7
Finite Difference Modeling and Parameter Estimation .....	9
Experimental Methods .....	11
Experimental Equipment .....	11
Phantom Tissue Tests .....	12
Exposed Rat Liver Tests .....	13
Results and Discussion .....	16
Phantom Tissue Model .....	16
Exposed Rat Liver Model .....	20
Conclusions .....	23
Acknowledgments .....	24
References .....	25
Thesis Conclusions and Future Recommendations .....	27
Overview of Phantom Tissue Test Results .....	27
Overview of Exposed Rat Liver Model Test Results .....	27
Recommendations for Future Work .....	27
Appendix A: Pressed Sensor Technology .....	29
Appendix B: Passive Perfusion Probe Finite Difference Model and Parameter Estimation .....	32

Finite Difference Formulation.....	32
Discretization of Governing Equation .....	33
Validation of Finite Difference Code.....	35
Parameter Estimation Procedure .....	37
Parameter Estimation Code.....	40
PassiveProbe_DriverProgram.m .....	41
Passive_ParameterEstimation.m .....	43
Passive_ExpDataFormatting.m .....	49
Passive_FDModel.m .....	52
Passive_SensitivityCoefficients.m .....	59
Passive_BloodPerfusion.m.....	60
Appendix C: LabVIEW VI.....	62
Appendix D: Experimental Data Analysis .....	65
Phantom Tissue Model Experimental Data.....	65
Statistical Analysis Summary .....	66
Phantom Tissue Model .....	66
Exposed Rat Liver Model.....	71
Appendix E: Data DVD.....	77

## List of Figures

Figure 1. The convective perfusion probe elicits a thermal response from tissue using compressed air.....	4
Figure 2. Heat flux sensor with laminated flat thermocouple. ....	6
Figure 3. Pressed sensor affixed to aluminum block, resulting in passive perfusion probe assembly.....	7
Figure 4. Schematic of finite difference model of tissue.....	10
Figure 5. Estimation method used to estimate blood perfusion, $\omega$ , and contact resistance, $R_c$ . ...	10
Figure 6. Data acquisition system used for phantom tissue and rat liver tests. ....	11
Figure 7. Three-dimensional model of phantom tissue test stand. ....	12
Figure 8. Phantom tissue test section with passive perfusion probe in place. ....	12
Figure 9. Exposed rat liver model experimental setup for convective perfusion estimation.....	15
Figure 10. Exposed rat liver model experimental setup for passive perfusion estimation. ....	15
Figure 11. Heat flux sensitivity for phantom tissue test stand.....	16
Figure 12. Average perfusion estimates with 95% confidence interval for all tests conducted on the phantom tissue test stand. ....	17
Figure 13. Comparison of the perfusion estimates for the convective, convective laminated, and passive perfusion probe experimental tests conducted on the phantom tissue test stand. ....	18
Figure 14. Perfusion estimates for all probes and Fluent CFD model for the phantom tissue test stand.....	19
Figure 15. Average contact resistance estimated for the passive perfusion probe for the phantom tissue model tests.....	20
Figure 16. Perfusion estimates for the exposed rat liver model with the passive perfusion probe. ....	21
Figure 17. Perfusion estimates for the exposed rat liver model with all probes.....	22
Figure 18. Schematic of thermocouple layout for spot welding.....	29
Figure 19. Spot welder used to manufacture thin film thermocouples.....	30
Figure 20. Schematic of Heat Flux Sensor with laminated foil thermocouple for hot press.....	30
Figure 21. Hot press used to manufacture heat flux sensor with laminated thin film thermocouple. ....	30
Figure 22. Heat Flux sensor with laminated thin film thermocouple. ....	31
Figure 23. Schematic of finite difference model . ....	32

Figure 24. Thermal circuit at the pressed sensor/tissue interface with contact resistance shown between them.....	33
Figure 25. Thermal resistances and heat flux calculations for Convective and Passive Perfusion Probes, as well as the adjustment made to the Passive Perfusion Probe. ....	36
Figure 26. Heat flux comparison of 2D Finite Difference for Convective and Passive Perfusion Probes.....	37
Figure 27. Plot of ideal objective function with parabolic shape and distinct minimum point at a given value of parameter being estimated. ....	38
Figure 28. Flowchart of the parameter estimation procedure using the whole domain method...	39
Figure 29. Flowchart of PassiveProbe_DriverProgram.m and incorporated Pennes Finite Difference Model and Parameter Estimation programs. ....	40
Figure 30. LabVIEW VI Front Panel used to record all experimental data. ....	63
Figure 31. LabVIEW VI Block Diagram used to record all experimental data. ....	64
Figure 32. Experimental perfusion results with 95% confidence intervals of the perfusion probes on the phantom tissue model. ....	65
Figure 33. Experimental and Fluent CFD perfusion results with 95% confidence intervals for the phantom tissue model tests.....	66
Figure 34. ANOVA Box plot for the passive perfusion probe on the phantom tissue model. ....	67
Figure 35. Multicomparison plot for the passive perfusion probe on the phantom tissue model. ....	67
Figure 36. ANOVA Box plot for the convective perfusion probe on the phantom tissue model..	68
Figure 37. Multicomparison plot for the convective perfusion probe on the phantom tissue model. ....	68
Figure 38. ANOVA Box plot for the convective laminated perfusion probe with convective code on the phantom tissue model.....	69
Figure 39. Multicomparison plot for the convective laminated perfusion probe with convective code on the phantom tissue model.....	69
Figure 40. ANOVA Box plot for the convective laminated perfusion probe with passive code on the phantom tissue model.....	70
Figure 41. Multicomparison plot for the convective laminated perfusion probe with passive code on the phantom tissue model.....	70
Figure 42. ANOVA Box plot for the passive perfusion probe (Day 1)on the exposed rat liver model.....	72
Figure 43. Multicomparison plot for the passive perfusion probe (Day 1) on the exposed rat liver model.....	72

Figure 44. ANOVA Box plot for the passive perfusion probe (Day 2) on the exposed rat liver model.....	73
Figure 45. Multicomparison plot for the passive perfusion probe (Day 2) on the exposed rat liver model.....	73
Figure 46. ANOVA Box plot for the convective perfusion probe on the exposed rat liver model.....	74
Figure 47. Multicomparison plot for the convective perfusion probe on the exposed rat liver model.....	74
Figure 48. ANOVA Box plot for the convective laminated perfusion probe with convective code on the exposed rat liver model.....	75
Figure 49. Multicomparison plot for the convective laminated perfusion probe with convective code on the exposed rat liver model.....	75
Figure 50. ANOVA Box plot for the convective laminated perfusion probe with passive code on the exposed rat liver model.....	76
Figure 51. Multicomparison plot for the convective laminated perfusion probe with passive code on the exposed rat liver model.....	76
Figure 52. Organization of attached DVD.....	77

## List of Tables

Table 1. Summary of the experimental procedure for the phantom tests. ....	13
Table 2. Summary of the experimental procedure for the exposed rat liver tests. ....	14
Table 3. Zero perfusion offsets for the phantom tissue model tests. ....	18
Table 4. Zero Perfusion Offsets for exposed rat liver tests. ....	22
Table 5. Average perfusion estimates for the exposed rat liver tests. ....	23
Table 6. Parameter values used for both the convective and passive finite difference models in comparison. ....	37
Table 7. Statistical analysis summary for the phantom tissue model. ....	66
Table 8. Statistical analysis summary for the exposed rat liver model. ....	71

## Nomenclature

### Nomenclature Used in Finite Difference Equations

$\alpha$	Thermal Diffusivity	$\Delta r$	Radial Distance Between Two Cells
$T$	Temperature ( $^{\circ}\text{C}$ )	$\Delta z$	Axial Distance Between Two Cells
$t$	Time (sec)	$q''$	Heat Flux ( $\text{W}/\text{m}^2$ )
$k$	Thermal Conductivity ( $\text{W}/\text{m}\cdot\text{K}$ )	$h$	Heat Transfer Coefficient ( $\text{W}/\text{m}^2\cdot\text{K}$ )
$\omega$	Blood Perfusion ( $\text{mL}/\text{mL}/\text{s}$ )	$j$	Node Index in Radial Direction
$R_c$	Contact Resistance ( $\text{m}^2\cdot\text{K}/\text{W}$ )	$i$	Node Index in Axial Direction
$r$	Radial Direction	$P$	Time Index
$z$	Axial Direction		

### Subscripts

$t$	Tissue	$nt$	Last Row of Cells in Tissue
$s$	Heat Flux Sensor	$mt$	Last Column of Cell in Tissue
$ps$	Pressed Heat Flux Sensor	$\infty$	Free Stream (Ambient)
$tl$	First Row of Cells in Tissue	$a$	Arterial

### Nomenclature Used In Parameter Estimation

$S$	Objective Function	$\beta$	Estimated parameter Vector
$\vec{q}''$	Vector of Heat Flux Values ( $\text{W}/\text{m}^2$ )	$b$	Approximation of $\beta$
$\vec{T}$	Vector of Temperature Values ( $^{\circ}\text{C}$ )	$\vec{X}$	Sensitivity Coefficient Vector
$\sigma$	Variance	$\Delta b$	Change in Parameter Estimate

### Subscripts

$m$	Measured	$q$	Heat Flux
$c$	Calculated	$T$	Temperature
$i$	Index		

### Superscripts

$k$	Iteration Number
$T$	Transpose

## **Preface**

This thesis is organized in a manuscript format that includes an individual research paper that documents the main focus of the work. The research paper includes an introduction and the objectives of the research project. A literature review of the past work and latest developments in blood perfusion measuring techniques are then presented. The research paper describes the design of the pressed sensor technology and passive perfusion probe design. The computational modeling involved in estimating perfusion is then explained. The experimental methods used for both the non-living and living tissue models are described in detail. Both the phantom tissue test stand and exposed rat liver models' results are presented and discussed. The paper concludes with overall conclusions for the passive perfusion probe. Future recommendations are then discussed. A series of appendices then follows which provide additional information on the pressed sensor technology, bioheat transfer model, the parameter estimation, finite difference model, experimental data acquisition, and experimental data analysis, all of which were used in the process of pursuing this research.

My role in the work presented here includes the development of the pressed sensor technology and passive perfusion probe design. The setup and experimental methods for the passive perfusion probe were an important focus of my research work. All of the experimental data included in this work were conducted by me or under my supervision. I programmed the acquisition of the experimental data through LabVIEW. Also, I performed all analysis of this experimental data shown in this work.

# **Non-Invasive Blood Perfusion Measurements Using a Combined Temperature and Heat Flux Surface Probe**

Patricia L. Ricketts<sup>1,2</sup>, Ashvinikumar V. Mudaliar<sup>1,2</sup>, Brent E. Ellis<sup>1,2</sup>, Clay A. Pullins<sup>2</sup>, Leah A. Meyers<sup>2</sup>, Otto I. Lanz<sup>1,3</sup>, Elaine P. Scott<sup>1,2,4</sup>, Thomas E. Diller<sup>1,2</sup>

<sup>1</sup>Virginia Tech – Wake Forest University School of Biomedical Engineering and Sciences

<sup>2</sup>Department of Mechanical Engineering, Virginia Tech

<sup>3</sup>Department of Small Animal Clinical Sciences, Virginia Tech

<sup>4</sup>Department of Engineering, Seattle Pacific University

## **Abstract**

A non-invasive blood perfusion system has been developed and tested in a phantom tissue and an animal model. The system uses a small sensor with a laminated flat thermocouple to measure the heat transfer response to an arbitrary thermal event (convective or conductive) imposed on the tissue surface. Blood perfusion and contact resistance are estimated by comparing heat flux data with a mathematical model of the tissue. The perfusion system was evaluated for repeatability and sensitivity using both a phantom tissue test stand and exposed rat liver tests. Perfusion in the phantom tissue tests was varied by controlling the flow of water into the phantom tissue test section, and the perfusion in the exposed liver tests was varied by temporarily occluding blood flow through the portal vein. The phantom tissue tests indicated that the probe can be used to detect small changes in perfusion (0.005 ml/ml/s). The probe qualitatively tracked the changes in the perfusion of the liver model due to occlusion of the portal vein.

## Introduction

Blood perfusion is the local, non-directional blood flow through living tissue. It is characterized as the volumetric flow rate of blood per volume of tissue. Blood perfusion is vital for normal tissue physiology and is responsible for the transport of oxygen, nutrients, and waste products. Also, blood perfusion is a principal part of the thermal regulatory system of the body. While it is related to the blood flow found in arteries and veins, there can be perfusion abnormalities in the presence of normal blood flow in the circulatory system.

Since blood perfusion is so important in maintaining normal physiologic conditions, the ability to measure blood perfusion has many clinical applications. A large range of perfusion values have been reported for human tissue (i.e. 0.002-0.5 ml/ml/s). This large range is thought to be due to measurement sensitivity, environmental factors, and tissue type and location. Variations in blood perfusion can indicate abnormal physiologic or pathologic conditions. These conditions include the assessment of skin graft acceptance, tumor growth, and burn and other wound healing. Therefore, the measurement of blood perfusion is a valuable medical diagnostic tool.

One promising method provides non-invasive perfusion estimates from a measured thermal response of the tissue. The Convective Perfusion Probe at Virginia Tech imposes a thermal event on a small area of tissue through convective cooling and measures the thermal response of the tissue using a small sensor [1]. Perfusion values are estimated by a minimization routine that compares the experimental heat flux measurements and those calculated from a corresponding mathematical model of the system. While the Convective Perfusion Probe has been shown to be a viable perfusion measurement probe, it is limited in application due to the required pressurized air supply.

The objective of the research by the blood perfusion group at Virginia Tech is to develop an inexpensive non-invasive blood perfusion probe that can be used in a number of clinical applications. The goals are to develop a version of the blood perfusion probe that has greater ease of use and validate this new probe using both phantom and animal tissue systems.

## Background on Perfusion Measuring Techniques

Both invasive and non-invasive methods have been developed to measure blood perfusion. Invasive methods include those techniques which require the insertion of a probe into the tissue. Some of these invasive methods require the placement of microspheres within the tissue to track flow changes [2] or measurement probes that deposit thermal energy into the tissue and measure the thermal response of the tissue [3]. These methods not only disturb the tissue to be measured, but also cause discomfort and increase the risk of infection to the patient.

Techniques for deep tissue perfusion measurements include imaging and some thermal methods. Magnetic Resonance Imaging (MRI) is among the non-invasive imaging methods used to directly measure blood perfusion by using arterial blood as an internal tracer [4]. Arterial Spin Labeling (ASL) is a MRI technique used to determine temporally and spatially resolved perfusion in tissue [5]. Williams et al. [6] used ASL to detect changes in rat brain perfusion using rats with hypercarbia, a condition that is known to increase brain perfusion, and those with freeze injuries, known to cause abnormalities in brain perfusion. While MRI provides accurate, repeatable and absolute perfusion measurements, it is limited to deep tissue [7], requires large, expensive equipment, and cannot be used in a surgical setting.

Positron Emission Tomography (PET) is another deep tissue imaging technique used to measure blood perfusion and requires that a radioactive tracer be introduced into the blood supply. A solution of glucose (sugar) that has been “tagged” with a radioactive chemical isotope (usually fluorine 18, N-ammonia, or O labeled water) is injected into the blood stream [8]. Metabolically active organs or tumors consume sugar at high rates, and as the “tagged” sugar begins to decay, positrons are emitted. These emitted positrons collide with electrons, giving off gamma rays, which a computer converts into images [9-10]. While this imaging technique also provides perfusion measurements, it is limited to deep tissue as well as the cost, size, and processing time of equipment.

A common technique for invasively measuring deep tissue blood perfusion uses a Thermal Diffusion Probe (TDP). This system works based on the clearance of thermal energy in the tissue [11, 12]. A thermal diffusion probe uses a self-heated thermistor to measure absolute perfusion in real time by measuring the power required to keep the probe temperature higher than the tissue temperature [3].

Laser Doppler Flowmetry (LDF) is a non-invasive surface measurement technique that has been established to provide real-time measurement of red blood cell motion within tissue. LDF and Laser Doppler Imaging (LDI) illuminate the tissue with a laser and perfusion is found from the product of the mean velocity and concentration of the red blood cells within the volume of tissue being measured [11]. Laser Doppler signals from the tissue are recorded in BPU (Blood Perfusion Units), a relative units scale calibrated using a suspension of latex spheres undergoing Brownian motion. They have previously been

used for monitoring dialysis [14], assessing the transplant rejection [15], and assessing the extent of burn wounds [16]. Several difficulties are associated with LDF technology. LDF inherently makes velocity measurements of red blood cells in one direction and only gives perfusion in relative values. These relative values were quantified by a simultaneous MRI ASL measurement of cerebral blood flow in rats by He et al. [17]. LDF is highly sensitive to the optical properties of the tissue.

Several non-invasive thermal methods have also been developed. These methods usually have a heater and temperature sensor on the surface of the tissue, arranged to minimize heat loss. Castellana et al. [18] placed a thin-film resistor on the skin surface to provide heat and measure the temperature. Holti and Mitchell [19] placed a thermopile between a heated copper piece and a surrounding piece of copper on the surface of the skin. They attempted to relate blood perfusion to the measured temperature difference established after several minutes of heating. These non-invasive thermal methods had limited success because of several problems. The heat losses to the ambient are typically large, making the actual heat flux going into the tissue difficult to determine. The thermal contact resistance between the probe and the surface of the tissue is important in non-invasive probes and can be difficult to determine.

The Convective Perfusion Probe at Virginia Tech was developed to overcome the problems encountered in the existing perfusion measuring systems as described above [20]. This probe, shown in Figure 1, used compressed air to cool the tissue and elicited a measurable heat flux response non-invasively. Unlike other probes, the heat flux response is measured directly from the tissue. This recorded heat flux, along with other measurable temperatures, was used to estimate perfusion through a finite difference model and parameter estimation routine. The convective perfusion probe's finite difference model was based on the measured air temperature within the housing, which created the measurable convective thermal event.

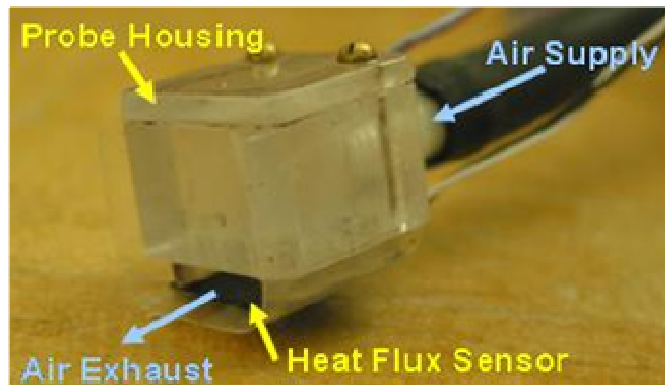


**Figure 1. The convective perfusion probe elicits a thermal response from tissue using compressed air.**

While this probe showed good sensitivity and repeatability for both living and nonliving tissue tests, its need for compressed air limits its clinical applications. The goal for this research was then to investigate other methods of providing the thermal event to simplify the system and improve its ease of use. A sensor system that could accurately and reliably estimate perfusion with a variety of thermal event sources, not just convection, was examined. The system was then tested on both non-living and living tissues and compared to performance of the previous convective probe. As before, this system should be safe, cost effective, operable in a variety of clinical environments (including surgery), non-invasive, and easy to use.

## Pressed Sensor Technology

Previously in the convective perfusion probe system, cooling was imposed on the tissue surface. The finite difference model of the convective perfusion probe was based on the recorded air temperature and heat flux. The resultant heat flux from the tissue was measured using a Vatell® model BF-02 heat flux gage. However, a temperature measurement was not provided at the location of the heat flux with this gage. To improve the setup, the sensor was modified by laminating a flat thermocouple to the side of the sensor in contact with the tissue.

A 0.0127mm (0.0005 inch) foil thermocouple (RDF Corporation) was laminated to the 10mm x 10mm heat flux sensor using layers of thin plastic and a heat activated epoxy. A layer of thin plastic was placed first, followed by a layer of heat activated epoxy, then the heat flux sensor. On the “tissue” side of the sensor, a layer of epoxy was applied, then a thin layer of plastic, another layer of epoxy, and then the foil thermocouple. A final layer of epoxy and thin plastic was then applied. This layered structure was placed in a hot press at 160°C for three hours. This resulted in a completely sealed sensor with a thin film thermocouple on the top of it. This laminated sensor provides a direct temperature measurement between the tissue and sensor, as well as a water tight seal to protect the sensor from moisture present in animal model tests. Figure 2 shows the sensor with laminated flat thermocouple.

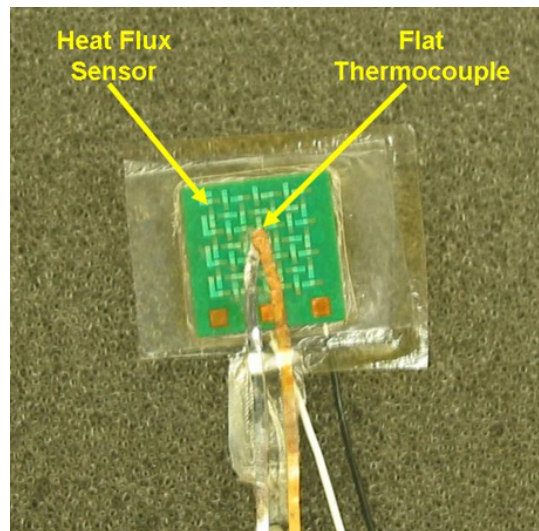


Figure 2. Heat flux sensor with laminated flat thermocouple.

## Perfusion Probe Design

With the pressed sensor technology, the source of the thermal event could be investigated and altered as needed. The pressed sensor provides continuous measurement of both the heat flux and

corresponding temperature at a given location. With both of these quantities continuously known, back solving could be used to find other parameters, such as perfusion. Therefore, the pressed sensor and altered finite difference code could estimate perfusion regardless of the mechanism used to elicit a heat flux response from the tissue.

### ***Convective Laminated Perfusion Probe***

The previously described convective probe [1,20] was adapted to incorporate the use of the pressed sensor. The pressed sensor with a laminated thin film thermocouple was attached to the probe housing instead of the original sensor without the thin film thermocouple. This adapted convective probe was then referred to as the Convective Laminated Perfusion Probe. With the addition of the pressed sensor, the finite difference model of the system was no longer confined to the use of air temperature alone. Now perfusion estimates could also be obtained using the heat flux and pressed thermocouple temperature measurements recorded directly from the tissue. In summary, the perfusion could be estimated in two ways: using the temperature of the air and its corresponding heat transfer coefficient, or using the heat flux and pressed thermocouple temperature recorded directly from the tissue.

### ***Passive Perfusion Probe***

Previously, convective cooling was used and required compressed air supply to operate the system. To improve upon that systems' portability, the Passive Perfusion Probe was developed. The passive probe utilizes a 10 mm cubic aluminum block to create the thermal event. The laminated sensor is affixed to one side of the aluminum block with double-sided tape, as shown in Figure 3.

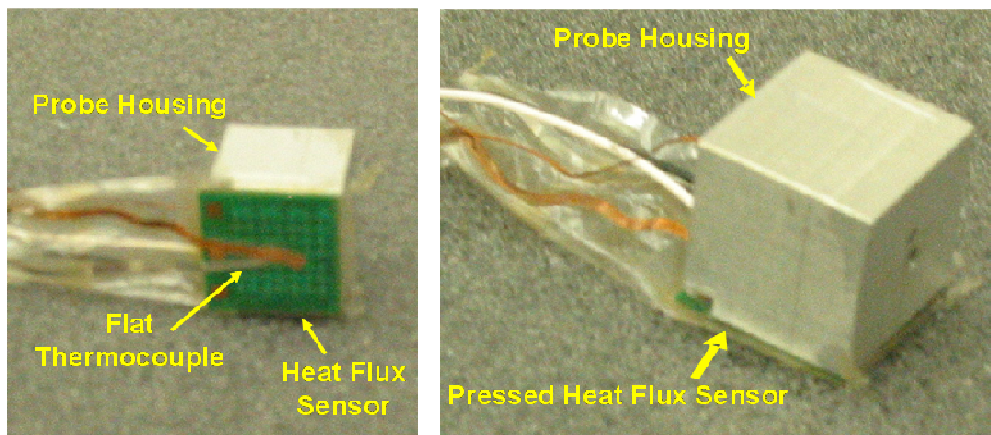


**Figure 3. Pressed sensor affixed to aluminum block, resulting in passive perfusion probe assembly.**

The system relies on the thermal capacitance of the block to provide the necessary difference in temperature to produce heat flux. Aluminum was chosen because the product of its conductivity, density, and specific heat is orders of magnitude larger than that of the tissue in the finite difference model. This large difference in thermal properties allows the aluminum to provide sufficient cooling for the tissue without causing discomfort to the patient. Also, aluminum is a readily available material that can be easily manufactured.

The assembly is then placed onto the tissue and the room temperature of the block elicits a heat flux response from the tissue. While the laminated thermocouple provides the sensor temperature, a thermistor is used to record the aluminum block's temperature during testing.

The Passive Perfusion Probe provides an adequate thermal event from which to estimate perfusion without requiring additional equipment or complicated modeling. Its simple and portable design allows it to be used widely in clinical and surgical situations.

## Finite Difference Modeling and Parameter Estimation

Perfusion is determined through parameter estimation techniques by comparing measured experimental and calculated heat flux data through a minimization routine [21]. A two dimensional cylindrical finite-difference model of the probe and tissue based on the Pennes [22] bioheat equation, neglecting metabolic heat generation, is used to attain the calculated heat flux data.

$$(\rho C_p)_t \frac{\partial T_t}{\partial t} = k_t \nabla^2 T_t + (\rho C_p \omega)_b (T_a - T_v) \quad (1)$$

where T is temperature, t is time,  $\rho$  is density,  $C_p$  is specific heat, k is thermal conductivity, and  $\omega$  is blood perfusion. The subscripts t, b, v, and a, correspond to tissue, blood, venous and arterial, respectively. The first term on the left hand side is the transient storage term. On the right hand side, conduction in the tissue makes up the first term followed by the term for energy loss due to blood flow. This equation is applied assuming that the tissue is homogenous, and is supplied with arterial blood at the body's core temperature. Also, the thermal properties of the tissue and blood are assumed to be constant; and the blood perfusion is assumed to be uniform throughout the tissue.

The input temperatures for the model include the recorded sensor, arterial and tissue temperatures. The heat flux and sensor temperature are recorded as functions of time throughout the thermal event. The arterial and tissue temperatures are averaged over the length of time prior to the start of the thermal event.

The boundary conditions of the model are shown in Figure 4. This finite difference model is simpler than previous models only in that it requires the sensor temperature as a boundary input. In this model the heat flux is calculated across the contact resistance. The model predicts perfusion and contact resistances regardless of the thermal event method used. Therefore, the pressed heat flux sensor and its model can be used with any perfusion probe.

An Alternating Directions Implicit (ADI) method is used to solve the discretized equations for the unknown temperature field. The Box-Kanemasu Method [21] is used to execute the minimization procedure as shown in Figure 5. Both perfusion and contact resistance at the interface between the probe and tissue are estimated. Contact resistance is independently estimated to eliminate the effects of differences in skin properties and surface characteristics.

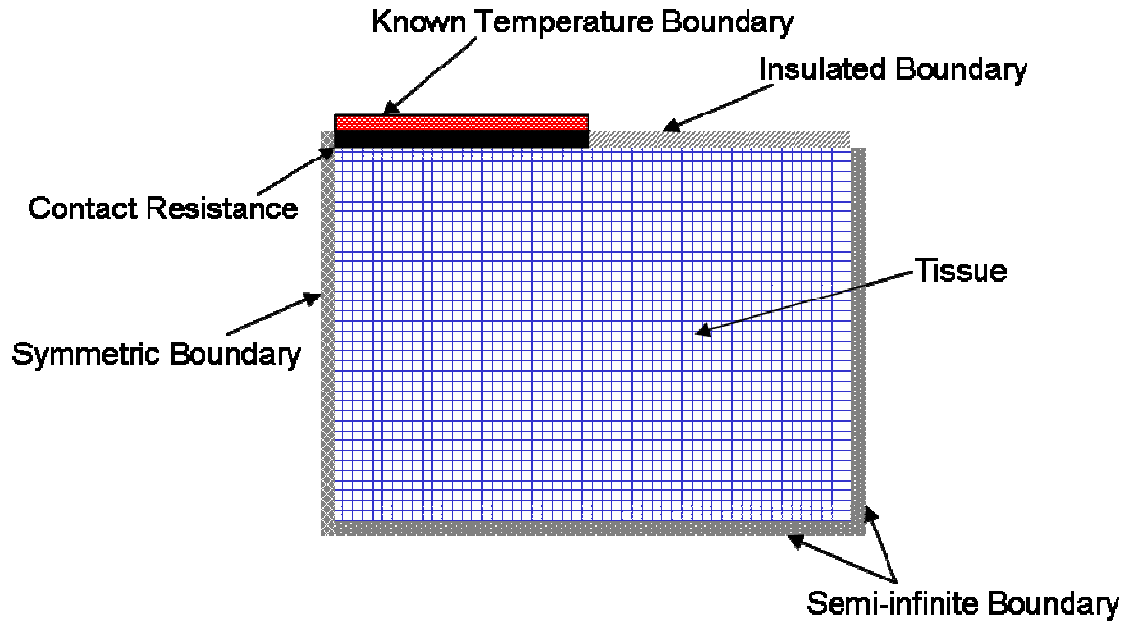


Figure 4. Schematic of finite difference model of tissue.

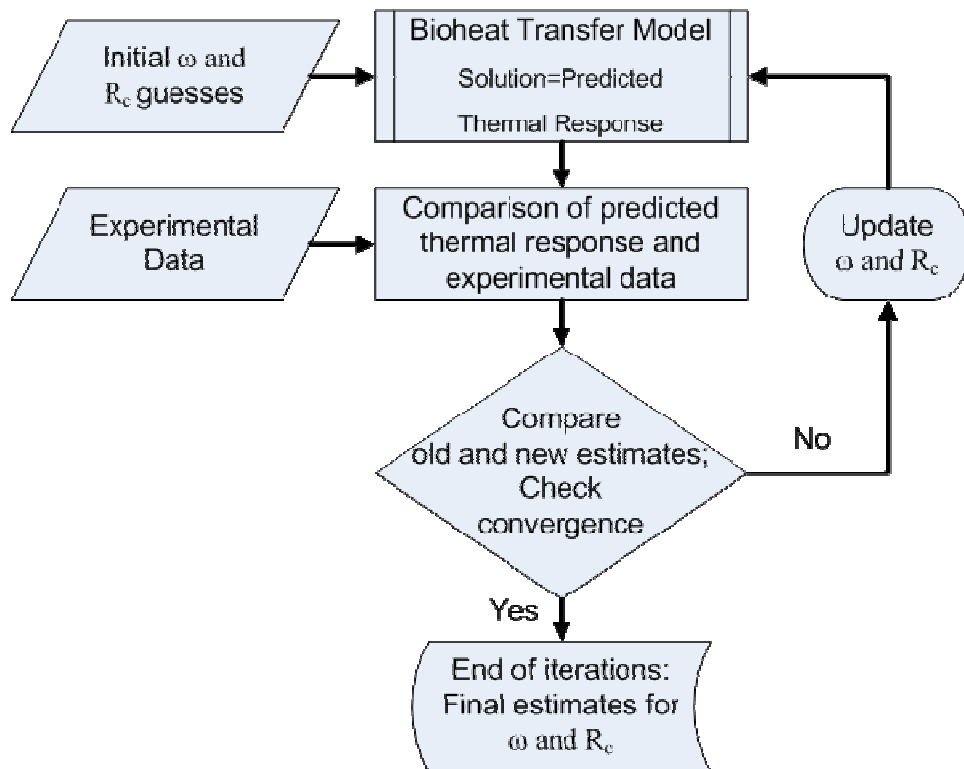


Figure 5. Estimation method used to estimate blood perfusion,  $\omega$ , and contact resistance,  $R_c$ .

## Experimental Methods

### *Experimental Equipment*

The heat flux and temperature data were recorded using the data acquisition system shown in Figure 6. The reference temperature for the thermocouple measurements is recorded using a Doric thermocouple reader. The signals from the heat flux sensor and the thermocouples were amplified, while the thermistor signals were not amplified. The thermistor signals were actuated by a voltage divider circuit that included a low-pass filter for each signal. All of these voltage signals were sampled at 12Hz with a 16 bit, USB high performance multifunction data acquisition system. Also, this multifunction data acquisition system provided the input voltage for the thermistor circuit. The data acquisition process was controlled through National Instruments LabVIEW 8.2 on a Pentium R-2GHz laptop.

The heat flux voltage measurement is converted to heat flux by multiplying by the sensor sensitivity provided by Vatel®. The thermocouple voltage measurements are converted to temperature by multiplying by the thermocouple sensitivity and adding the reference temperature. The thermistor resistance measurements are converted to voltage using a voltage divider and low-pass filter circuit. These voltage measurements are then converted to temperature using a polynomial equation obtained from the thermistor calibration data sheet. All of the above conversions are programmed into a NI LabVIEW VI so that the output is a text file containing only time, heat flux, and temperature measurements.

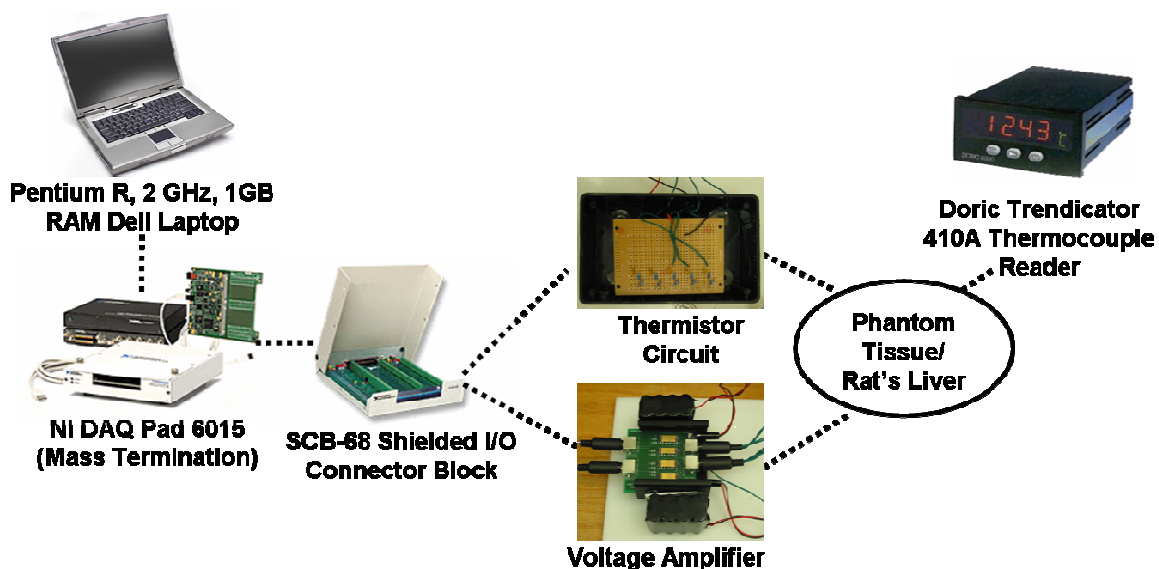
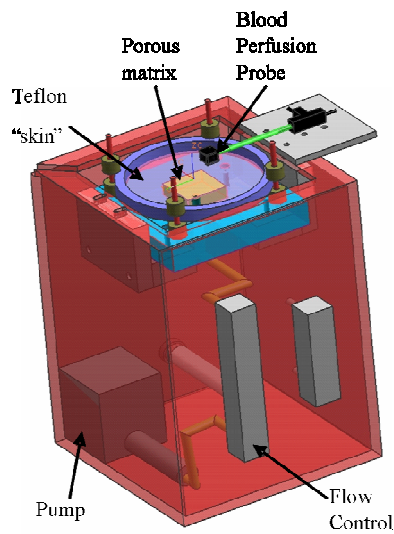


Figure 6. Data acquisition system used for phantom tissue and rat liver tests.

### **Phantom Tissue Tests**

A three-dimensional drawing of the phantom tissue test stand [20] is shown in Figure 7. This test stand allows for a wide range of known, repeatable perfusion flows while eliminating physiological uncertainty. The phantom tissue test stand provides a controlled environment for perfusion estimation tests and minimizes animal usage. The test stand consists of a porous matrix (sponge) positioned directly above an inlet of water controlled by a flow meter. The entire test section is enclosed in a water bath maintained at the core body temperature of 37°C. Figure 8 shows the assembled phantom tissue test stand in operation with the passive perfusion probe. This test has been validated computationally and experimentally with previous perfusion probes by the group at Virginia Tech [20].



**Figure 7. Three-dimensional model of phantom tissue test stand.**

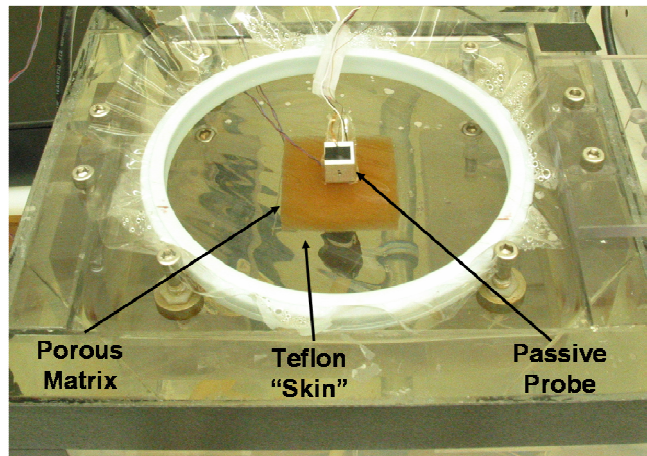


**Figure 8. Phantom tissue test section with passive perfusion probe in place.**

Table 1 summarizes the experimental procedure timeline that was used for all phantom tissue tests. First, the flow rate is set and the system is allowed to equilibrate. Data acquisition begins and the first minute of data acquisition is used to determine the offset in the heat flux signal. Next, the thermal event is initiated after sixty seconds and continues for the second minute of data acquisition. Finally, the porous matrix is flushed at the maximum flow rate for two minutes to equilibrate the temperature within the porous matrix. After the two minutes of flushing, the procedure is repeated.

**Table 1. Summary of the experimental procedure for the phantom tests.**

<b>Step</b>	<b>Convective Procedure (Both Convective and Convective Laminated Perfusion Probes)</b>	<b>Passive Procedure</b>	<b>Time</b>
1	Set desired flow rate for the experimental runs	Set desired flow rate for the experimental runs	Prior to test run
2	Start the data acquisition (heat flux and temperature)	Start the data acquisition (heat flux and temperature)	0 sec
3	Turn the air supply on	Place the probe on the tissue	60 sec
4	Turn the air supply off	Remove the probe from the tissue; Return probe to aluminum plate	120 sec
5	Set the flow meter to maximum flow	Set the flow meter to maximum flow	125 sec

Tests were completed for flow rates ranging from 0cc/min to 30cc/min in increments of 5cc/min. At each flow rate, twelve tests were completed to test the repeatability of the test stand.

### ***Exposed Rat Liver Tests***

To validate the perfusion probe's use on living tissue, an exposed liver of an anesthetized rat was used as a model. First the surgical procedure used to prepare the rats is presented. Then the convective perfusion probe's experimental procedure is discussed, followed by that of the passive perfusion probe.

The rat was anesthetized and maintained under general anesthesia with isoflurane in 100% oxygen. Once anesthetized, the ventral abdomen was clipped from the xiphoid to the pubis and aseptically prepared for surgery. A sheet of ioban was used to drape the surgical site and an incision was made from the xiphoid to the pubis using a number 15 scalpel blade. The portal vein was then identified and isolated for further manipulation. Occlusion of portal blood flow to

the liver was temporarily performed using a microvascular clamp placed over the portal vein. The hepatic artery was not occluded at any time during the experimental procedure. To re-establish portal blood flow the microvascular clamp was removed from the portal vein.

Table 2 summarizes the experimental procedure timeline that was used for all exposed rat liver tests. First, the portal vein condition is set (occluded or non-occluded). Data acquisition begins and the first minute of data acquisition is used to determine the offset in the heat flux signal. Next, the thermal event is initiated after sixty seconds and continues for the second minute of data acquisition. Finally, the tissue is flushed by removing the occlusion and reestablishing portal blood flow within the tissue. After the two minutes of reestablished blood flow, the procedure is repeated.

**Table 2. Summary of the experimental procedure for the exposed rat liver tests.**

<b>Step</b>	<b>Convective Procedure (Both Convective and Convective Laminated Perfusion Probes)</b>	<b>Passive Procedure</b>	<b>Time</b>
1	Set desired portal vein condition (occluded or non-occluded)	Set desired portal vein condition (occluded or non-occluded)	Prior to test run
2	Start the data acquisition (heat flux and temperature)	Start the data acquisition (heat flux and temperature)	0 sec
3	Turn the air supply on	Place the probe on the tissue	60 sec
4	Turn the air supply off	Remove the probe from the tissue; Return probe to aluminum plate	120 sec
5	Remove occlusion and reestablish portal blood flow within tissue	Remove occlusion and reestablish portal blood flow within tissue	125 sec

The first two tests were done without occluding the vein to ensure the repeatability of the measured heat flux data from the blood perfusion probe. The subsequent eight tests were conducted by alternately occluding the portal vein and then removing the clamp. Clamping the portal vein insures that blood flow both in and out of the tissue is ceased.

During all tests, the arterial and tissue temperatures were recorded with both thermocouples and thermistors. The arterial temperature of the rat was taken as the abdominal cavity temperature. The tissue temperature was taken as the temperature of liver lobe on which the probe was placed. The tissue temperature also provided an initial temperature for the numerical model.

During both the convective and convective laminated perfusion probes tests, the air temperature was recorded within the probe housing. The placement of the convective perfusion probe on the liver is shown in Figure 9. During the passive perfusion probe tests, the pressed thermocouple temperature was recorded. The cubic aluminum block's temperature was recorded using a thermistor and monitored to ensure the block returned to 26°C between experimental test runs. The placement of the passive perfusion probe on the liver is shown in Figure 10.

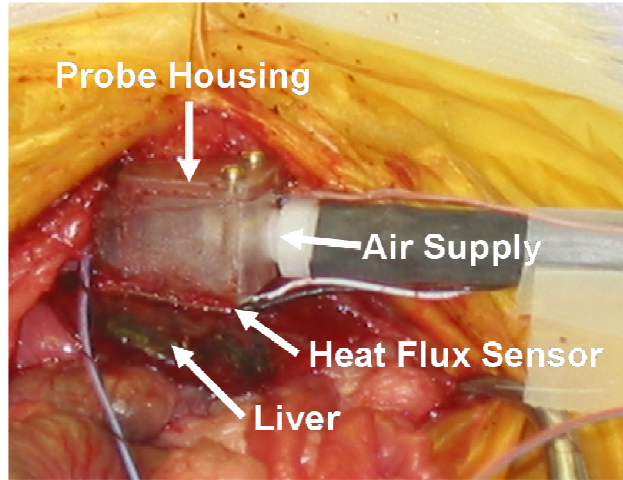


**Figure 9. Exposed rat liver model experimental setup for convective perfusion estimation.**

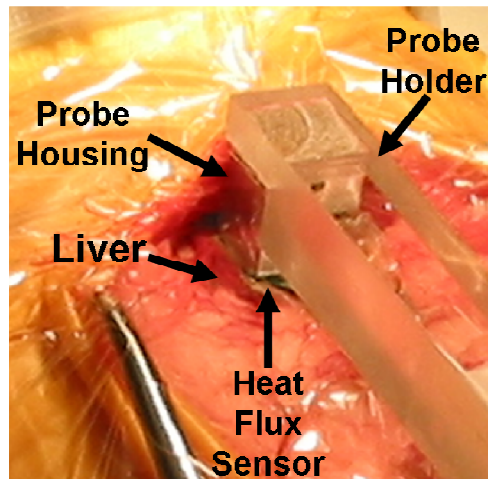


**Figure 10. Exposed rat liver model experimental setup for passive perfusion estimation.**

## Results and Discussion

Results for both the phantom tissue model and the exposed rat liver model are discussed here. These results include both the experimental heat flux and parameter estimates perfusion and contact resistance.

### *Phantom Tissue Model*

The phantom tissue test stand was designed to eliminate physiological uncertainty and produce repeatable results. A goal of the passive perfusion probe was the ability to repeatedly distinguish between various flow rates on the phantom tissue test stand. Figure 11 shows that the passive perfusion probe was able to consistently detect changes in perfusion. This figure displays distinctly different trends for the different flow rates. These trends were expected and correlate to different perfusion values. This resulting sensitivity of the probe to a change in flow rate is directly related to its sensitivity to a change in perfusion.

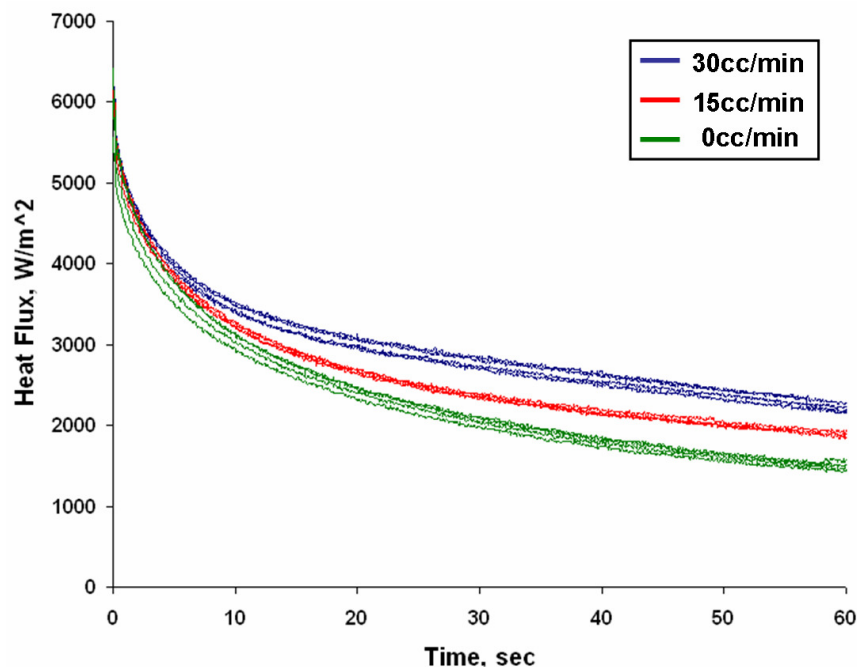
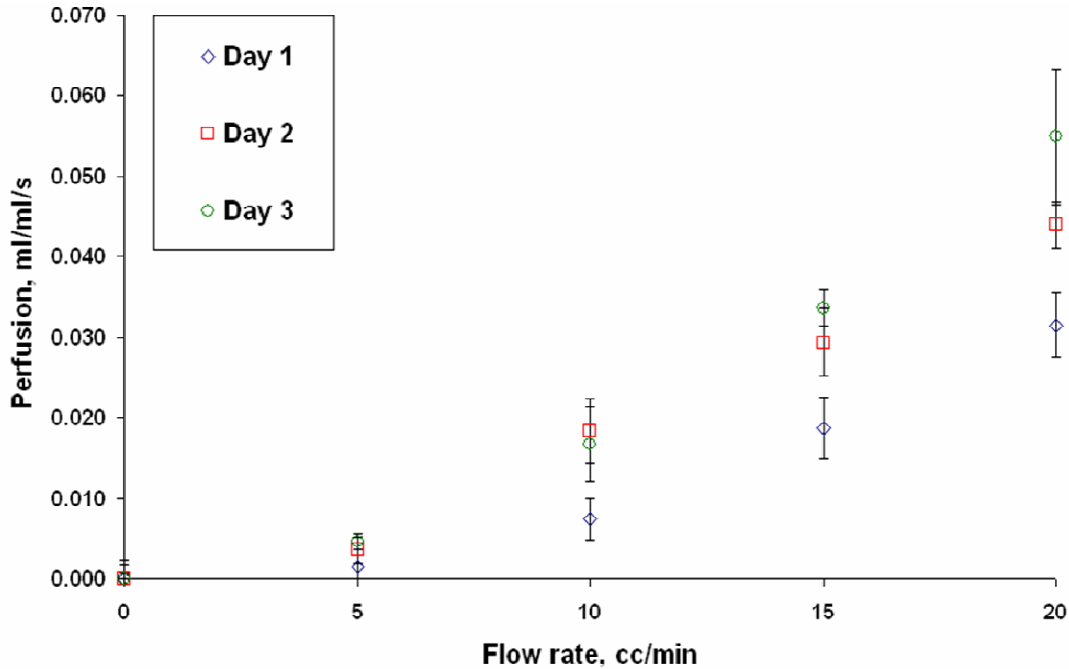


Figure 11. Heat flux sensitivity for phantom tissue test stand.

The parameter estimation code discussed previously was used to determine the experimental perfusion in the phantom tissue test stand for all tests at each flow rate. The average experimental perfusion values with 95% confidence interval for three days of testing for flow rates ranging from 0 to 20cc/min in 5cc/min increments are shown in Figure 12. While data was collected at higher flow rates of 25 and 30cc/min, they were not included since those flow rates are not seen in physiological tissue. From

the fact that all three days of testing result in the same trend, it can be deduced that the passive perfusion probe displays measurement repeatability. While the variation between measurements is much smaller for the lower flow rates, it increases for the higher flow rates.



**Figure 12. Average perfusion estimates with 95% confidence interval for all tests conducted on the phantom tissue test stand.**

The overall average of the convective, convective laminated and passive perfusion probes results with 95% confidence interval is shown in Figure 13. Note that the convective laminated results were obtained with two versions of the finite difference code: the convective and passive codes. The convective code models the convection above the sensor with the measured air temperature and given heat transfer coefficient. The passive code uses the model previously discussed with only the measured pressed thermocouple temperature.

The perfusion estimates at 0cc/min were slightly above or below zero for each probe. To adjust for this, the perfusion estimates at 0cc/min were averaged and then referred to as the zero perfusion offset for each probe. These zero perfusion offsets for each probe were then subtracted from all tests in each set of probe data, resulting in a perfusion of zero at 0cc/min. A summary of these zero perfusion offsets is given in Table 3.

All probe results are in good agreement; however the passive probe's uncertainties are notably higher than the other probes. This prompted a statistical analysis of the means of each probe. The means of the convective perfusion probe's perfusion results for flow rates of 0-20cc/min were found to be

statistically different from one another. This is also true for the convective laminated probe's perfusion results, for both the convective and passive codes. The passive probe's perfusion means were not statistically different from one another for flow rates of 0-20cc/min. For all probes, the probability that the perfusion means for flow rates of 0-20cc/min will not be equal is a hundred percent.

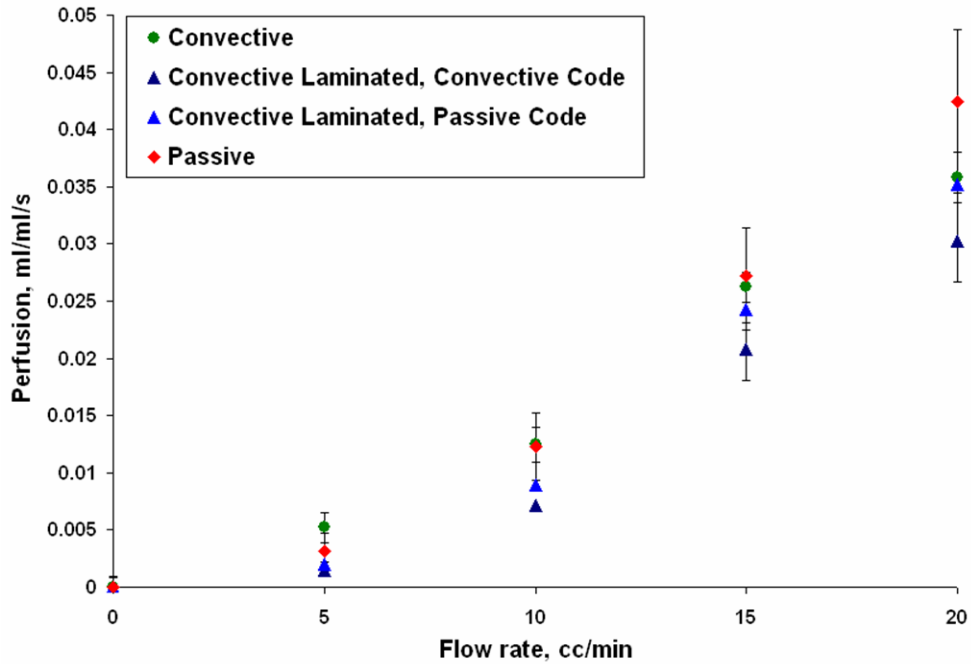


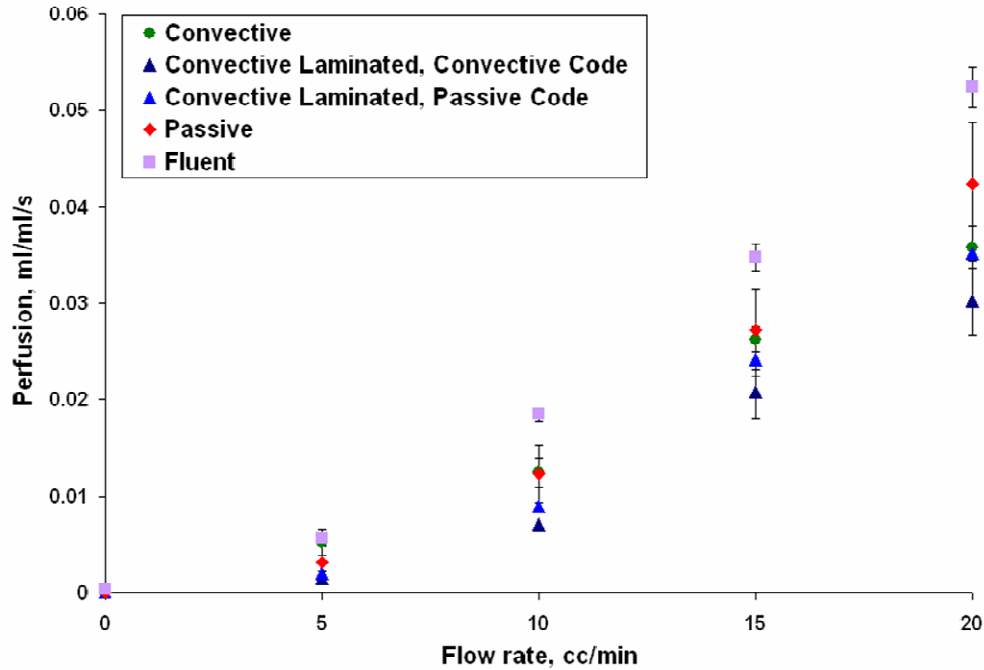
Figure 13. Comparison of the perfusion estimates for the convective, convective laminated, and passive perfusion probe experimental tests conducted on the phantom tissue test stand.

Table 3. Zero perfusion offsets for the phantom tissue model tests.

Probe	Zero Perfusion Offset (ml/ml/s)
Convective Probe	0.00122
Convective Laminated Probe Air Code	-0.00380
Convective Laminated Probe Passive Code	-0.00364
Passive Probe	0.00613

A comparison of the experimental results with the results of a computational fluid dynamics model of the tissue during the thermal event [20], all with 95% confidence intervals, is shown in Figure 14. Because the perfusion probes and tissue phantom are square, both three and two dimensional models

were initially developed. Since both models resulted in very close perfusion estimates, the 2D model was used to conserve computational time [20]. It can be seen that the CFD Model's results are higher than those of the perfusion probes at all flow rates. However, all of the results show a proportional trend between flow rate and perfusion.



**Figure 14. Perfusion estimates for all probes and Fluent CFD model for the phantom tissue test stand.**

The average contact resistances estimated for the passive perfusion probe on the phantom tissue model with the 95% confidence intervals are shown in Figure 15. It can be seen from this figure that there is no correlation between contact resistance and flow rate. The convective and convective laminated perfusion probes displayed similar trends for contact resistance estimates.

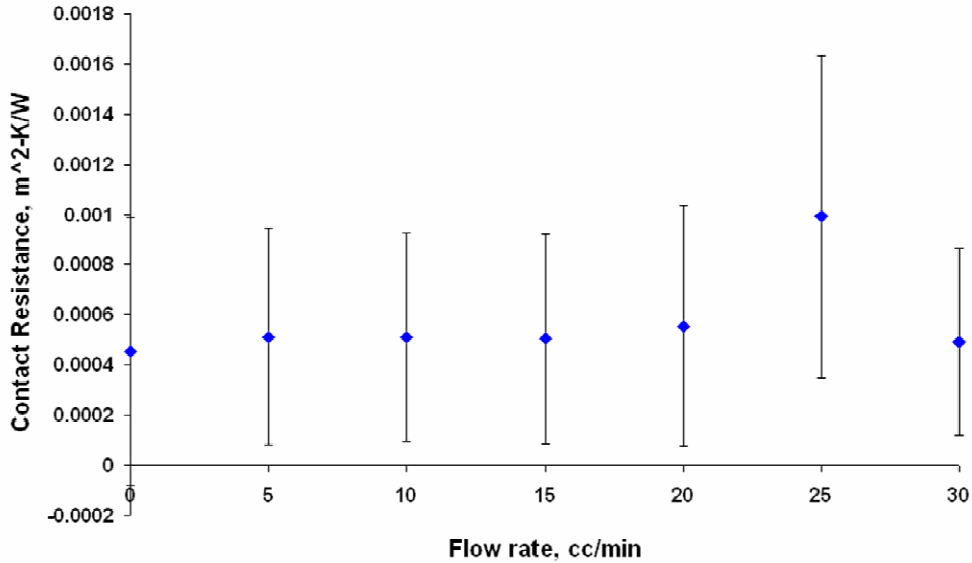


**Figure 15. Average contact resistance estimated for the passive perfusion probe for the phantom tissue model tests.**

Overall, these results visibly indicate the relationship between flow rate and perfusion. The convective laminated probe is shown to accurately estimate perfusion with both the convective and passive finite difference models. These results provide both an experimental and theoretical validation of the passive perfusion probe for obtaining perfusion estimates. All of the perfusion probes are shown to estimate contact resistance without the influence of flow rate.

### ***Exposed Rat Liver Model***

*In vivo* tests were conducted using the liver model to evaluate the qualitative performance of the passive perfusion probe. The heat flux response was similar to that seen on the phantom tissue test stand. The exposed rat liver model's parameter estimation results for two days of testing are shown in Figure 16. As with the phantom tissue test stand model, each day of testing resulted in a slight offset in perfusion values. These zero perfusion offsets were calculated by averaging the perfusion estimates for occluded tests (Tests 3, 5, 7 and 9). These offsets were then subtracted from all of the tests for each data set, resulting in near zero perfusion for the occluded cases. The zero perfusion offsets for the first and second data sets of passive perfusion probe tests were -0.01413 and -0.01019 ml/ml/s, respectively. The perfusion estimates show good repeatability for the initial cases (before occlusion). The subsequent tests exhibit the effects of occluding the portal vein. The perfusion drops substantially, as expected, for the occluded cases. Also as expected, the non-occluded cases have perfusion values similar to those before occlusion.

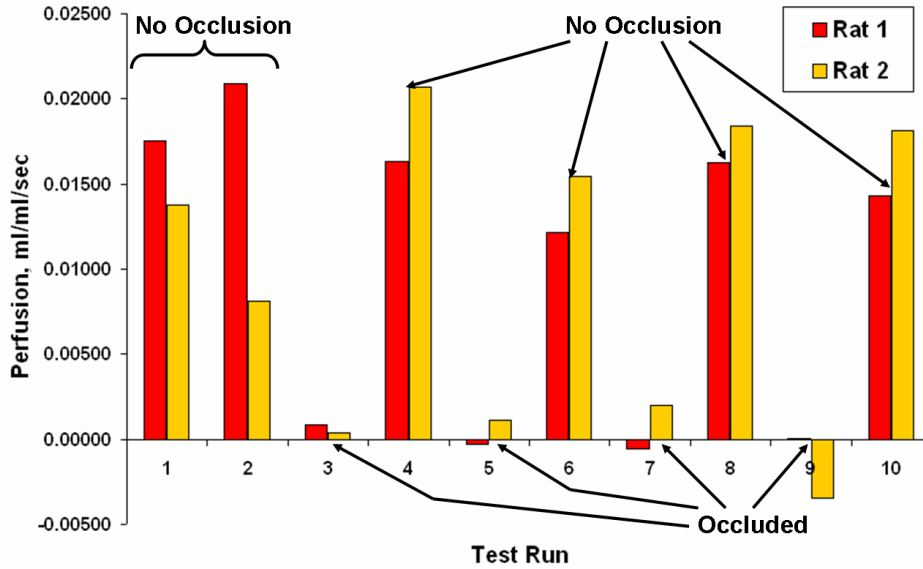


**Figure 16. Perfusion estimates for the exposed rat liver model with the passive perfusion probe.**

To further validate the passive perfusion probe’s ability to predict perfusion values in living tissue, the previous results were compared to results obtained from other perfusion probes during the same testing regimen. The summary of these results are shown in Figure 17. The first set of data is that obtained with the convective perfusion probe. The second and third sets of data were obtained with the convective laminated perfusion probe. The addition of the pressed sensor allowed perfusion to be estimated from the same data set by two methods: the convective perfusion probe’s parameter estimation routine and the passive perfusion probe’s parameter estimation routine. This difference in data processing is noted as the convective code and passive code in the figure’s legend. The fourth and fifth sets of data are the passive perfusion probe results previously discussed.

As discussed previously, the occluded cases resulted in non-zero perfusion estimates. To account for this, the perfusion estimates of the occluded cases (Tests 3, 5, 7 and 9) were averaged and subtracted from all results for each probe. Table 4 lists each of the zero perfusion offsets subtracted from the exposed rat liver tests for each probe. Table 5 lists the average perfusion estimates for the initial, occluded and non-occluded cases for all probes. Statistical analysis showed that the initial, occluded and non-occluded means for each probe presented in Table 5 are statistically different from one another. Therefore the probability that the means of the cases will be equal is less than a tenth of a percent. Therefore the probes were able to reliably distinguish perfusion changes between the initial, occluded, and non-occluded cases.

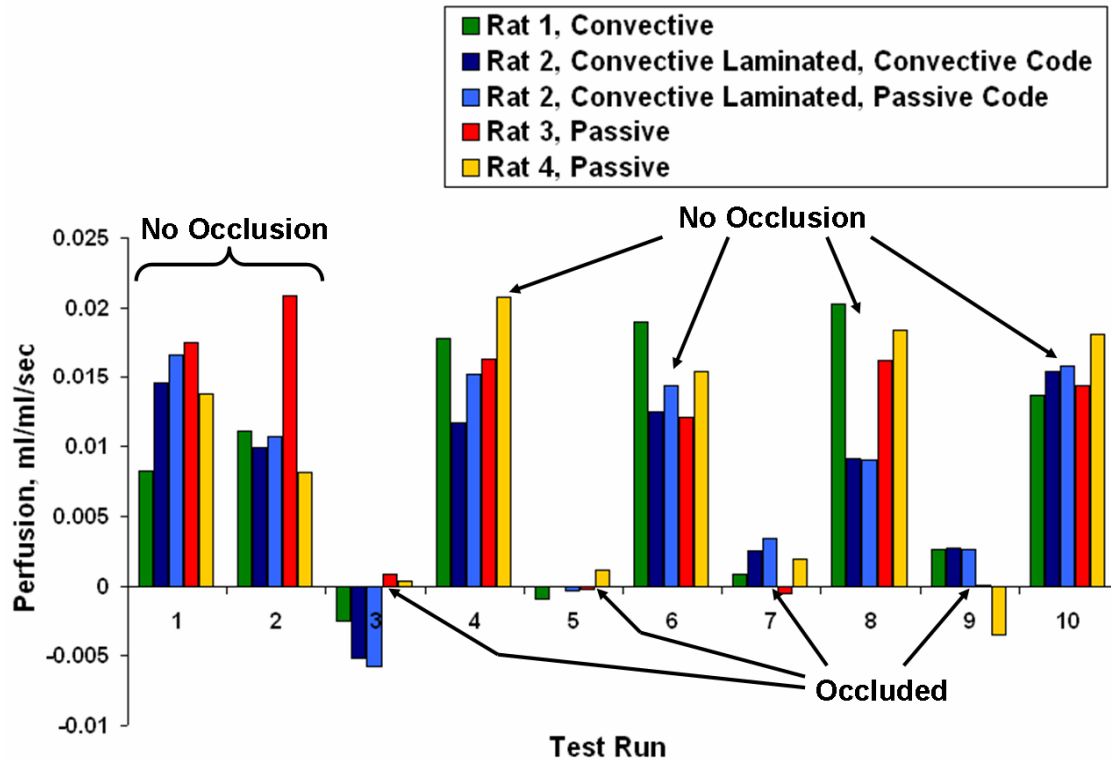


Figure 17. Perfusion estimates for the exposed rat liver model with all probes.

Table 4. Zero Perfusion Offsets for exposed rat liver tests.

Probe	Zero Perfusion Offset (ml/ml/s)
Convective Probe	0.00088
Convective Probe with Pressed Sensor Air Code	0.00198
Convective Probe with Pressed Sensor Passive Code	-0.00471
Passive Probe Day 1	-0.01413
Passive Probe Day 2	-0.01019

**Table 5. Average perfusion estimates for the exposed rat liver tests.**

<b>Probe</b>	<b>Average Perfusion (ml/ml/s)</b>		
	<b>Initial (Before Occlusion)</b>	<b>Occluded</b>	<b>Non- Occluded</b>
Convective Probe	0.00965	0.00000	0.01767
Convective Laminated Convective Code	0.01226	0.00000	0.01220
Convective Laminated Passive Code	0.01368	0.00000	0.01364
Passive Day 1	0.01920	0.00000	0.01475
Passive Day 2	0.01095	0.00000	0.01818

## Conclusions

The performance of the passive perfusion probe was effectively shown on both a non-living and a living tissue model. All of the tests with the passive perfusion probe displayed good repeatability and sensitivity. Tests on the phantom tissue model showed that the passive perfusion probe could detect changes in perfusion of 0.009 ml/ml/s increments over a range of 0-20cc/min. While the passive probe's means at each of these flow rates were not statistically different from one another, the passive perfusion probe's results were similar to those of the convective and convective laminated perfusion probes. The means of the convective and convective laminated probes were statistically different for flow rates of 0-20cc/min. For all probes, the probability that the perfusion means for flow rates of 0-20cc/min will be equal is zero percent.

The rat liver was used as an experimental model to provide living tissue characteristics. The passive perfusion probe qualitatively measured perfusion changes in the rat liver caused by the occlusion of the portal vein. Again, the passive perfusion probe's results were statistically different from one another for the initial, occluded and non-occluded cases. The convective and convective laminated probes' perfusion estimates were also found to be statistically different for the initial, occluded and non-occluded cases on the rat liver model. Therefore the probability of that the means of the initial, occluded and non-occluded cases will be equal is less than a tenth of a percent for all probes. These results demonstrate that the passive perfusion probe can quantitatively and qualitatively measure perfusion non-invasively.

## **Acknowledgments**

This work has been supported by Grant No. EP03943-01 from the National Institutes of Health.

## References

1. Mudaliar, A.V., Ellis, B.E., Ricketts, P.L., Lanz, O.I., Lee, C.Y., Scott, E.P., Diller, T.E., “Non-Invasive Blood Perfusion Measurements of an Isolated Rat Liver and an Anesthetized Rat Kidney”, Submitted to Journal of Biomechanical Engineering.
2. Prinzen, F. W., and J. B. Bassingthwaite, 2000, “Blood flow distributions by microsphere deposition methods,” Cardiovascular Research, Vol. 45, pp. 13-21.
3. Khot. M. B., P. K. M. Maitz, B. R. Phillips, H. F. Bowman, J. J. Pribaz, D. P. Orgill, 2005, “Thermal Diffusion Probe Analysis of Perfusion Changes in Vascular Occlusions of Rabbit Pedicle Flaps,” Plastic Reconstructive Surgery., Vol. 115, No. 4, pp. 1103-1109.
4. Montet, X., Ivancevic, M.K., Belenger, J. Jorge-Costa, M., Pochon, S., Pechér, A., Terrier, F., Vallé, J., 2003, “Noninvasive measurement of absolute renal perfusion by contrast medium enhanced magnetic resonance imaging”, Investigative Radiology, Vol. 38, No.9, pp. 584-592.
5. Vallee, J.P., Lazeyras, F., Khan, H.G., et al., 2000, “Absolute blood flow quantification by dynamic MRI and Gd-DTPA”, European Radiology, Vol. 10, No. 8, pp. 1245-1252.
6. Willams, D.S., Detre, J.A., Leigh, J.S., Koretsky, A.P., 1992, “Magnetic resonance imaging of perfusion using spin inversion of arterial water”, Proceedings of the National Academy of Sciences of the United State of America, Vol. 89, pp. 212-216.
7. Dias, M., Hadgraft, J., Glover, P.M., McDonald, P.J., 2003, “Stray Field Magnetic Resonance Imaging: A Preliminary Study of Skin Hydration”, J. Phys, Vol. 36, pp. 364-368.
8. Schelbert, Heinrich R., 2000, “PET Contributions to Understanding Normal and Abnormal Cardiac Perfusion and Metabolism.” Annals of Biomedical Engineering, Vo. 28, pp 922-929.
9. Nuutila, P. and K. Kalliokoski, 2000, “Use of positron emission tomography in the assessment of skeletal muscle and tendon metabolism and perfusion,” Scandinavian Journal of medicine & Science in Sports Vol. 10, pp. 346-350.
10. Boellaard, R., P. Knaapen, A. Rijbroek, G. J. J. Lutersema, A. A. Lammertsma, 2005, “Evaluation of Basis Function and Linear Least Squares Methods for Generating Parametric Blood Flow Images Using 15O-Water and Positron Emission Tomography” Molecular Imaging and Biology.
11. Valvano, J.W., J.T. Allen, H.F. Bowman, 1984, “The Simultaneous Measurement of Thermal Conductivity, Thermal Diffusivity, and Perfusion in Small Volumes of Tissue,” Journal of Biomechanical Engineering, Vol. 106, pp. 192-197.
12. Bowman, H., 1985, “Estimation of Tissue Blood Flow,” in: Heat Transfer in Medicine and Biology, eds. A. Shitzer and R. Eberhart, Vol. 1, Chap. 9, Plenum Press, pp 193-203.

13. Svedman, C., G.W. Cherry, E. Strigini, T.J. Ryan, 1998, "Laser Doppler Imaging of Skin Microcirculation," *Acta Dermato-Venereologica*, Vol. 78, pp. 114-118.
14. Niwayama, J., and T. Sanaka, 2005, "Development of a new method for monitoring blood purification: The blood flow analysis of the head and foot by laser Doppler blood flow meter during hemodialysis," *Hemodialysis International*, Vol. 9, pp. 55-62.
15. Oltean, M. A. Aneman, G. Dindelegan, J. Mölne, M. Olausson, and G. Herlenius, 2005, "Monitoring of the Intestinal Mucosal Perfusion Using Laser Doppler Flowmetry After Multivisceral Transplantation," *Transplantation Proceedings*, Vol.37, pp 3323-3324.
16. Mileski, W. J. L. Atilas, G. Purdue, R. Kagan, J. R. Saffle, D. N. Herndon, D. Heimbach, A. Luterman, R. Yurt, C. Goodwin, J. L. Hunt, 2003, "Serial Measurements Increase the Accuracy of Laser Doppler Assessment of Burn Wounds," *Journal of Burn Care & Rehabilitation*, Vol. 24, pp. 187-191.
17. He, J., Devonshire, I.M., Mayhew, J.E.W., Papadakis, N.G., 2007, "Simultaneous laser Doppler flowmetry and arterial spin labeling MRI for measurement of functional perfusion changes in the cortex," *NeuroImage*, Vol. 34, pp. 1391-1404.
18. Castellana, F.S., Skalak, R., Cho, J.M., Case, R.B., 1983, "Steady State Analysis and Evaluation of New Thermal Sensor for Surface Measurement of Tissue Perfusion", *Annals of Biomedical Engineering*, Vol. 11, pp. 101-115.
19. Holti, G. and Mitchell, K.W., 1979, "Estimation of the Nutrient Skin Blood Flow using a Non-Invasive Segmented Thermal Clearance Probe", *Non-Invasive Physiological Measurements*, edited by E.P. Rolfe, Vol. 1, Chap. 5, Academic Press, London, pp. 113-123.
20. Mudaliar, A.V., Ellis, B.E., Ricketts, P.L., Lanz, O.I., Scott, E.P., Diller, T.E., "A Phantom Tissue System for the Calibration of a Perfusion System", Submitted to *Journal of Biomechanical Engineering*.
21. Scott, E.P., Robinson, P.S., and Diller, T.E., 1998, "Development of Methodologies for the Estimation of Blood Perfusion Using a Minimally Invasive Probe", *Measurement Science and Technology*, (Invited Paper – Special Edition), Vol 9, No. 6, pp. 888-897.
22. Pennes, H. H., 1948, "Analysis of Tissue and Arterial Blood Temperatures in the Resting Human Forearm," *J. Appl. Physiol.*, Vol. 1, pp. 93-122.

## **Thesis Conclusions and Future Recommendations**

Blood perfusion is a principal component in the thermoregulatory system of the body and vital for normal tissue physiology. The ability to measure blood perfusion is a valuable medical diagnostic, as perfusion abnormalities can indicate of a number of physiologic or pathologic problems.

### ***Overview of Phantom Tissue Test Results***

The phantom tissue system proved to be a convenient, reliable test bed for surface perfusion measurements in an environment where physiological and pathological conditions are eliminated. The phantom tissue system was shown to be valid with a combination of experimental and CFD results. The passive perfusion probe was shown to be sensitive and repeatable for perfusion measurements. The contact resistance calculated by the parameter estimation program is important but is generally independent of the flow rates. The repeatability, sensitivity and good comparison with the CFD model and experimental results proves that change in perfusion can be monitored by the passive perfusion probe.

### ***Overview of Exposed Rat Liver Model Test Results***

The passive perfusion probe qualitatively assessed the perfusion changes in the rat liver caused by the occlusion of the portal vein. The repeatability, sensitivity, and good agreement with the animal model results demonstrate that perfusion can be qualitatively and quantitatively measured by the passive perfusion probe.

### ***Recommendations for Future Work***

#### *Recommendations for the phantom experiments*

In order to improve the passive perfusion probe's resolution of 0.009ml/ml/s on the phantom tissue test stand, testing could be performed at smaller increments. All the tests presented in this work were conducted at an increment of 5cc/min, by decreasing the increment interval to 2 or 3 cc/min the resolution may be improved. Also, the experimental procedure could be examined to improve the temperature measurements. Sensitivity analysis showed that the finite difference model and parameter estimation routine are extremely sensitive to the input temperature. During testing user errors or outside disturbances may cause fluctuations in these temperature measurements. Therefore, by improving these measurements the estimates may be improved.

### *Probe Design Recommendations*

The passive probe was designed to use the thermal capacitance of the block to cool the tissue. For this initial passive perfusion probe, aluminum was chosen due to its wide availability and its thermal capacitance being much higher than that of the tissue. Other materials could be investigated for the probe's construction. For example, copper has a much higher density than aluminum; however its specific heat is lower. The material which provides the ideal thermal capacitance for the tissue-probe interface could be examined.

Also, the passive perfusion probe could be further validated by utilize a simple geometry change. Currently the passive perfusion probe is oriented so that the thin film thermocouple is placed between the tissue and the sensor. This allows perfusion estimates to be obtained using the passive code, which only models the thin film thermocouple input at the skin's surface. By flipping the laminated heat flux sensor over, so that the thin film thermocouple is placed between the sensor and the aluminum block, the previously validated convective code could be used to estimate perfusion. This geometry change would allow known temperature boundary and sensor to be modeled accurately as in the original convective code use. Ideally the results of these two orientations would be close to one another, therefore validating the operating principal of the passive perfusion probe with the convective code.

## Appendix A: Pressed Sensor Technology

The Vatell<sup>®</sup> heat flux sensor is laminated with a thin film thermocouple in order to 1) provide the direct skin-sensor interface temperature measurement and 2) seal the sensor to prevent any damage from moisture during animal testing. The sensor is hot pressed using a thermally activated epoxy from the John C. Dolph company. While the epoxy cures, the hot press eliminates as many air bubbles as possible. First, the thin film thermocouples are manufactured. The 0.0127 mm (0.0005 inch) Type T thermocouple material (copper and constantan) is laid out in the configuration shown in Figure 18. The thermocouple material is spot welded at the junction using the welder shown in Figure 19. To only weld at the apex of the thermocouple layout, the junction is placed between the electrodes of the welder and only enough current to weld at this point is applied.

The heat flux gage and thin film thermocouple are cleaned with Acetone to remove any greases, oils or other substances that many have accumulated on them. Then the sensor and flat thermocouple are layered into an assembly as shown as in Figure 20. Mylar of 0.014986 mm (0.00059 inch) thickness is a thin plastic film used to encapsulate both the sensor and the thermocouple. Kapton<sup>®</sup> tape is used at all corners to keep the Mylar taut. To reduce the number of air bubbles within the pressing, the entire assembly is sandwiched between pyramids of Teflon. This forms an impression in which the air bubbles are forced into and away from the sensor and thermocouple surfaces. The assembly is pressed at 160°C for 3 hours in the hot press shown in Figure 21. After the pressed assembly has cooled, the excess Mylar is trimmed. Figure 22 shows the final product of hot pressing: a sealed heat flux sensor with a laminated heat flux sensor.

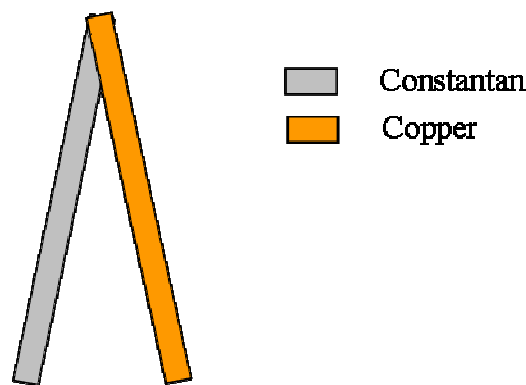


Figure 18. Schematic of thermocouple layout for spot welding.



Figure 19. Spot welder used to manufacture thin film thermocouples.

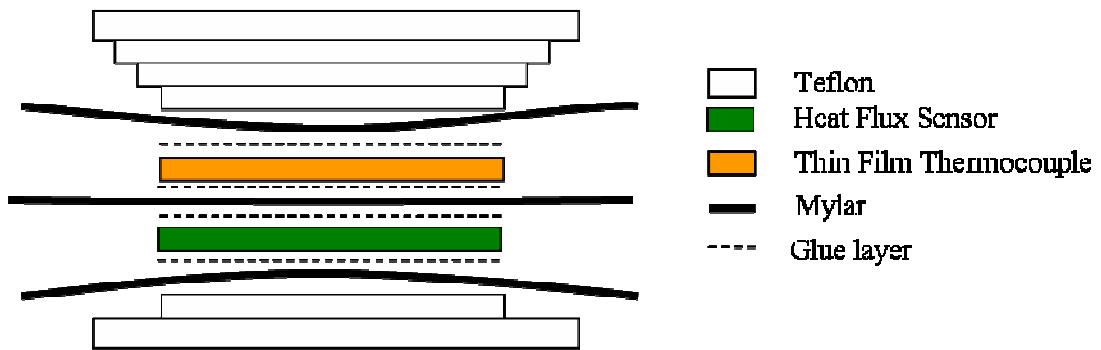
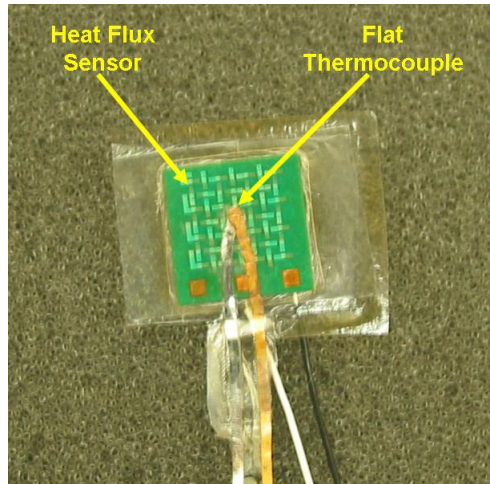


Figure 20. Schematic of Heat Flux Sensor with laminated foil thermocouple for hot press.



Figure 21. Hot press used to manufacture heat flux sensor with laminated thin film thermocouple.



**Figure 22. Heat Flux sensor with laminated thin film thermocouple.**

## Appendix B: Passive Perfusion Probe Finite Difference Model and Parameter Estimation

### *Finite Difference Formulation*

To solve the Pennes bioheat equation, a two dimensional finite difference solution was used. Due to simplicity, a cylindrical coordinate system was chosen. Figure 23 shows a schematic of the finite difference model. An Alternating Directions Implicit (ADI) method was used to solve the discretized equation for the unknown temperature field. The heat flux was calculated across the contact resistance continuously. The pressed sensor temperature for the known temperature boundary was recorded continuously as well. The arterial and initial tissue temperatures were calculated by averaging the respective temperature measurements prior to the start of the thermal event. The initial temperature within the finite difference model was set as the gradient between the arterial temperature at the bottom of the model and the initial tissue temperature at the top of the model.

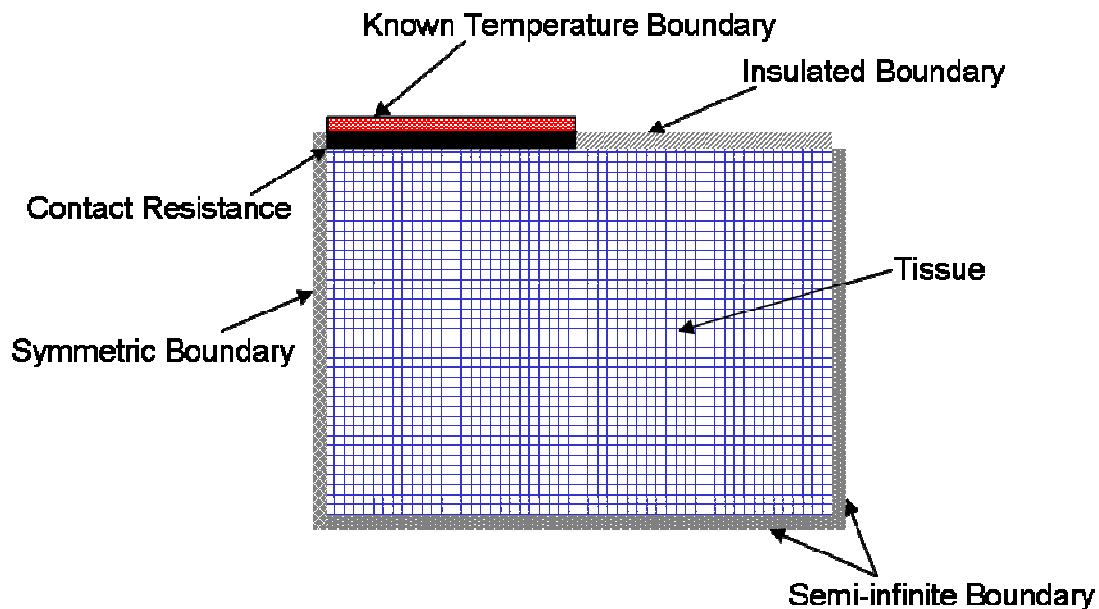


**Figure 23. Schematic of finite difference model .**

A driver program was developed to run the parameter estimation routine and save all of the perfusion, contact resistance, sum of squares, and convergence plots for each file. Since each file contains the actual heat flux and temperature values, no conversion is needed within the parameter estimation code. Also, the parameter estimation code detects the start and end of the thermal event based on the experimental heat flux file.

The boundary conditions for the passive perfusion code are calculated using imaginary cells at the symmetric, insulated and semi-infinite boundaries. At the known temperature boundary and the interface between the tissue, the thermal resistance concept shown in Figure 24 was used.

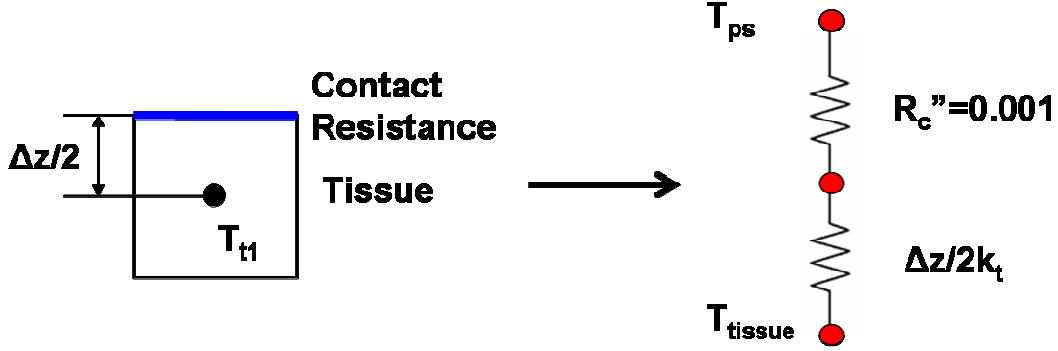


**Figure 24. Thermal circuit at the pressed sensor/tissue interface with contact resistance shown between them.**

Both the Pennes bioheat equation and the probe governing equation were fully discretized by integrating each term in space and time. For example:

$$\int_{r=0}^{r_{\max}} \int_{z=0}^{z_{\max}} \int_p^{p+1} \frac{\partial T(r, z, t)}{\partial t} dt dz dr = \quad (B.1)$$

$$\int_{r=0}^{r_{\max}} \int_{z=0}^{z_{\max}} \int_p^{p+1} \left[ \frac{1}{r} \frac{\partial}{\partial r} \left( r \frac{\partial T(r, z, t)}{\partial r} \right) + \frac{\partial^2 T(r, z, t)}{\partial z^2} + \omega(T_a - T(r, z, t)) \right] dt dz dr$$

A Crank-Nicolson implicit method was used to achieve the time discretization. In this method a linear variation between the temperature at the present time and the temperature at the next time step is assumed, as shown in Equations B.2 and B.3. Equation B.2 applies to the left hand side of Equation B.1, while Equation B.3 applies to the right hand side of Equation B.1.

$$\frac{\partial T}{\partial t} = \frac{T^{p+1} - T^p}{\Delta t} \quad (B.2)$$

$$\int_p^{p+1} T_{i,j} dt = \left( \frac{1}{2} T_{i,j}^{p+1} + \frac{1}{2} T_{i,j}^p \right) \Delta t \quad (B.3)$$

### **Discretization of Governing Equation**

The resulting finite difference equations from the numerical discretization are shown here

Energy equation in the tissue (Pennes bioheat equation)

$$\frac{\partial T}{\partial t} = \alpha_t \left( \frac{1}{r} \frac{\partial T}{\partial r} + \frac{\partial^2 T}{\partial r^2} \right) + \alpha_t \left( \frac{\partial^2 T}{\partial z^2} \right) + \omega(T_a - T)$$

Axial sweep in tissue

$$A_{1t} T_{i-1,j}^{n+\frac{1}{2}} + B_{1t} T_{i,j}^{n+\frac{1}{2}} + A_{1t} T_{i+1,j}^{n+\frac{1}{2}} = \\ C_{1t}(j) T_{i,j-1}^n + D_{1t} T_{i,j}^n + E_{1t}(j) T_{i,j+1}^n + \frac{\omega \Delta t}{2} T_a^n$$

Boundary conditions for axial sweep in tissue

ContactResistance

$$T_{t1,j}^{n+\frac{1}{2}} \left( 1 + \frac{k_t}{\Delta z} \left( R_c'' + \frac{\Delta z}{2k_t} \right) \right) - T_{t1+1,j}^{n+\frac{1}{2}} \frac{k_t}{\Delta z} \left( R_c'' + \frac{\Delta z}{2k_t} \right) = T_{ps,j}^n$$

Insulated Boundary

$$T_{t1,j}^{n+\frac{1}{2}} = T_{t1+1}^{n+\frac{1}{2}}$$

Semi – infinite Boundary (zero heat flux)

$$T_{nt,j}^{n+\frac{1}{2}} = T_{nt-1,j}^{n+\frac{1}{2}}$$

Radial sweep in tissue

$$C_{1t}(j) T_{i,j-1}^{n+1} + D_{2t} T_{i,j}^{n+1} + E_{1t}(j) T_{i,j+1}^{n+1} = \\ -A_{1t} T_{i-1,j}^{n+\frac{1}{2}} + B_{2t} T_{i,j}^{n+\frac{1}{2}} - A_{1t} T_{i+1,j}^{n+\frac{1}{2}} + \frac{\omega \Delta t}{2} T_a$$

Boundary conditions for radial sweep in tissue

Symmetric Boundary

$$T_{i,1}^{n+1} = T_{i,2}^{n+1}$$

Semi - infinite Boundary

$$T_{i,mt}^{n+1} = T_{i,mt-1}^{n+1}$$

where

$$A_{1t} = \left[ -\frac{\alpha_t \Delta t}{2 \Delta z^2} \right]$$

$$B_{1t} = \left[ 1 + \frac{\alpha_t \Delta t}{\Delta z^2} + \frac{\omega \Delta t}{2} \right]$$

$$B_{2t} = \left[ 1 + \frac{\alpha_t \Delta t}{\Delta r^2} + \frac{\omega \Delta t}{2} \right]$$

$$C_{1t} = \left[ \frac{\alpha_t \Delta t}{2 \Delta r} \left( \frac{1}{\Delta r} - \frac{1}{2r(j)} \right) \right]$$

$$D_{1t} = \left[ 1 - \frac{\alpha_t \Delta t}{\Delta r^2} \right]$$

$$D_{2t} = \left[ 1 - \frac{\alpha_t \Delta t}{\Delta z^2} \right]$$

$$E_{1t} = \left[ \frac{\alpha_t \Delta t}{2 \Delta r} \left( \frac{1}{\Delta r} + \frac{1}{2r(j)} \right) \right]$$

### ***Validation of Finite Difference Code***

The results from the passive probe finite difference model needed to be validated against the convective probe finite difference model. In order to compare the two finite difference models, the thermal resistances over which the heat flux is calculated were made equal. Figure 25 shows the thermal resistance circuits for both probes prior to equilibration. From this diagram, it can be seen that the total resistance between the convective and passive probes differed by a factor of two additional resistances. In order to account for this difference, the passive probe's thermal resistance was adjusted to match that of the convective. This was done by adding the convective resistance and sensor resistance to the contact resistance already in the model. This change is shown on the far right of Figure 25. After this adjustment, the finite difference models were ran

using the thermal properties shown in Table 6. The heat flux comparison obtained from these models is shown in Figure 26 and demonstrates a good agreement between the models. The slight disagreement seen in the heat flux curves is due to the difference in heat flux calculations between the convective and passive finite difference models. For the convective probe, the heat flux is calculated across the thickness of the sensor, therefore incorporating the thermal capacitance of the sensor. For the passive probe, the heat flux is calculated between the pressed sensor node and the first node in the tissue, thus not including the heat flux sensor's thermal capacitance into the model.

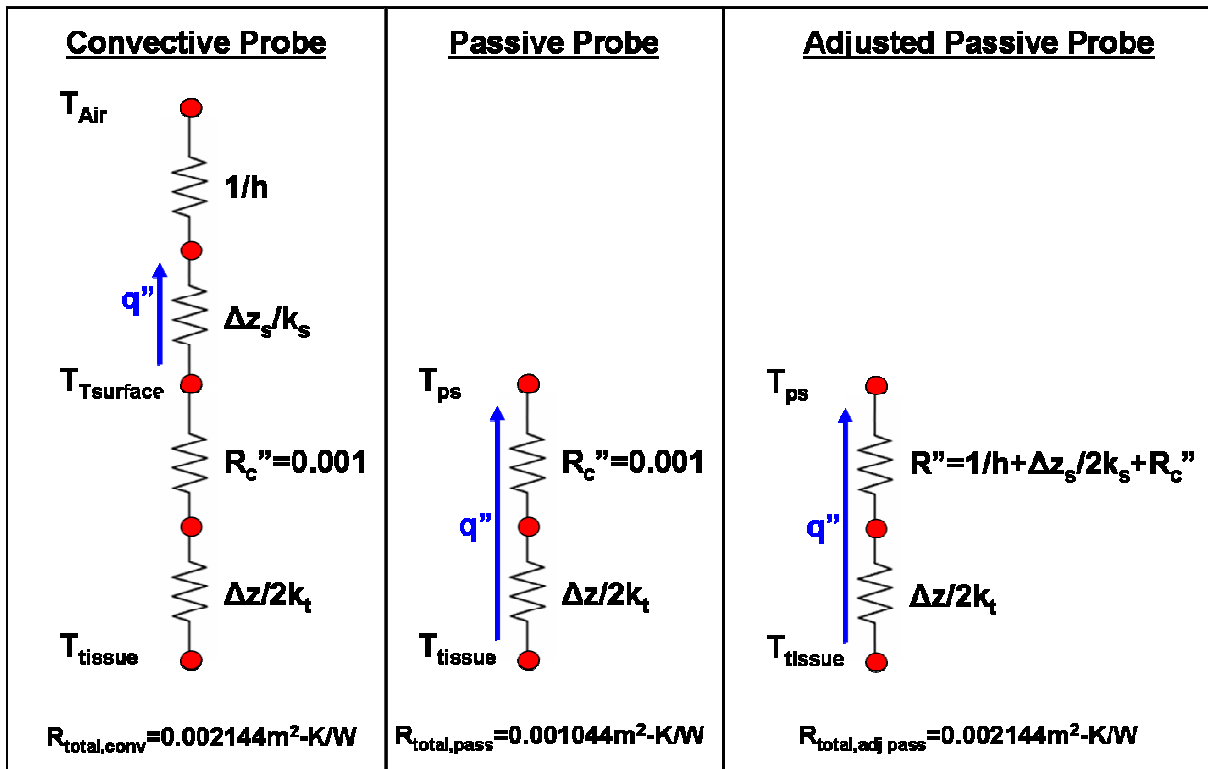
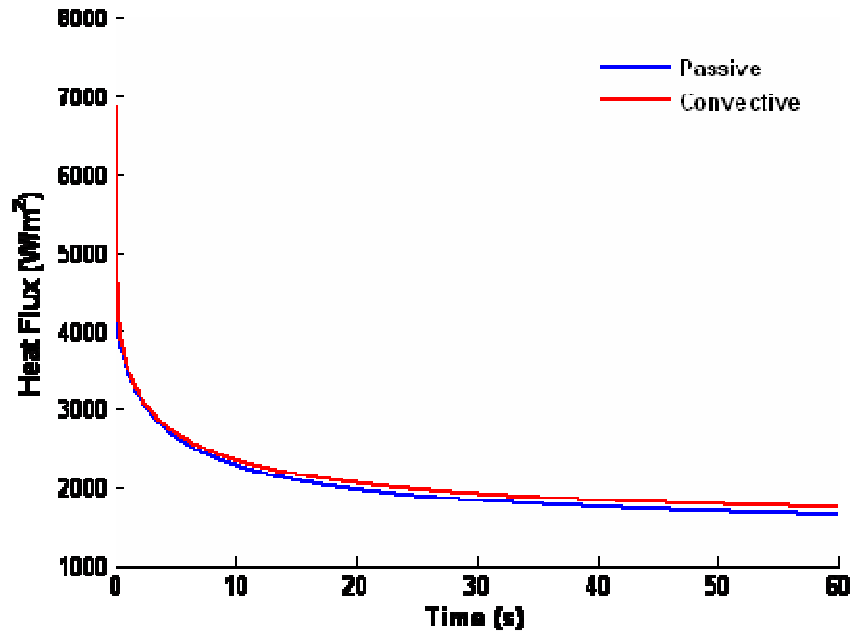


Figure 25. Thermal resistances and heat flux calculations for Convective and Passive Perfusion Probes, as well as the adjustment made to the Passive Perfusion Probe.

**Table 6. Parameter values used for both the convective and passive finite difference models in comparison.**

Parameter	Value	Probe
Tart	36°C	Both
Ttop	35°C	Both
$\omega$	0.002 ml/ml/s	Both
$R_c''$	0.001 m <sup>2</sup> -K/W	Both
Tair	25°C	Convective
h	10000 W/m <sup>2</sup> -K	Convective
Tsurf	25°C	Passive



**Figure 26. Heat flux comparison of 2D Finite Difference for Convective and Passive Perfusion Probes.**

### ***Parameter Estimation Procedure***

The thermal analysis parameter estimation program is based on Gauss minimization with Box-Kanemasu modification. This method adjusts the model parameters to obtain an optimum match between the experimental data and the model output. In order to achieve this match, an objective function that relates the experimental and model data is minimized. The objective function used is a sum of squares error between the measured and calculated data:

$$S = \sum_{i=1}^N \frac{(\bar{q}_{m_i}'' - \bar{q}_{c_i}'')^2}{\bar{\sigma}_q^2} \quad (\text{B.4})$$

Where  $q''$  denotes heat flux. The subscripts  $m$  and  $c$  denote measured and calculated, respectively.  $\sigma_q^2$  denotes the variance of the experimental heat flux.

Ideally, the objective function would show a parabolic shape with one distinct minimum point ideally, as shown in Figure 27. When the slope of the objective function is relatively flat, insensitivity occurs. When multiple minimums exist, non-uniqueness occurs.

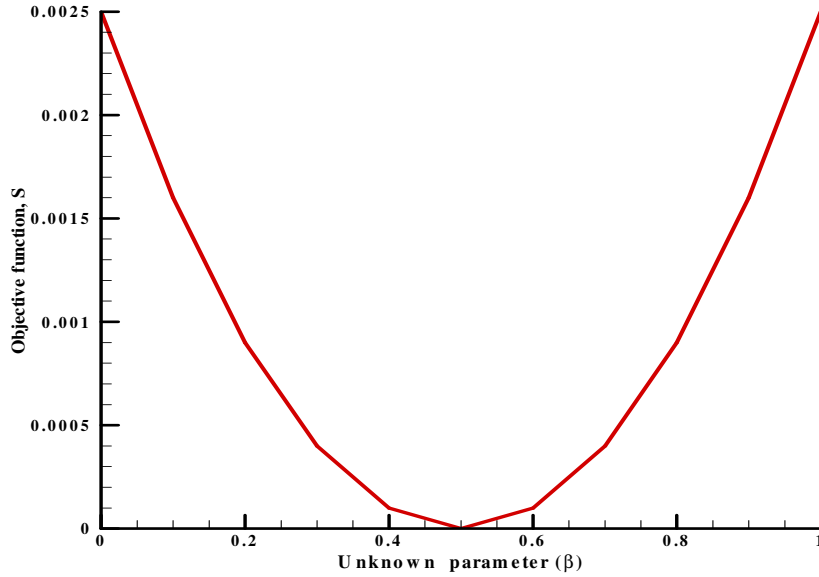


**Figure 27. Plot of ideal objective function with parabolic shape and distinct minimum point at a given value of parameter being estimated.**

The minimum value of the objective function is found by setting the derivative of  $S$  with respect to the estimated parameter vector,  $\beta$ , to zero in the Gaussian method. For the objective function shown previously in equation B.4, this process yields:

$$\nabla_{\beta} S = \frac{2}{\bar{\sigma}_q^2} (-\nabla_{\beta} \bar{q}_c''(\beta))^T (\bar{q}_m'' - \bar{q}_c''(\beta)) \quad (\text{B.5})$$

where  $\nabla_{\beta} \bar{q}_c''(\beta)$  is defined as the sensitivity vector for heat flux,  $\bar{X}_q(\beta)$ . Two approximations are made at this point. First, the sensitivity vector,  $\bar{X}_q(\beta)$  is approximated as  $\bar{X}_q(\bar{b})$ , where the vector,  $\bar{b}$  is an approximation of  $\beta$ . For this analysis, the vector  $\bar{b}$  includes the estimates of perfusion and contact resistance. Second,  $\bar{q}_c''(\beta)$  is approximated as the first two terms of a Taylor series expansion about  $\bar{b}$ . To solve for the next parameter estimates,  $\beta = \bar{b}^{k+1}$ , given the

previous values,  $\bar{b} = \bar{b}^k$ , the approximations explained previously are substituted into equation B.5. This step yields

$$\bar{b}^{k+1} = \bar{b}^k + \Delta\bar{b}^k \quad (\text{B.6})$$

where  $\Delta\bar{b}^k$  is given by

$$\Delta\bar{b}^k = \left( \frac{1}{\bar{\sigma}_q^2} \bar{X}_q(\bar{b})^T \bar{X}_q(\bar{b}) \right)^{-1} \cdot \left( \frac{1}{\bar{\sigma}_q^2} \bar{X}_q(\bar{b})^T (\bar{q}_m'' - \bar{q}_c''(\bar{b})) \right) \quad (\text{B.7})$$

These Gauss iterative estimates continue until the parameter convergence is reached or until the maximum number of iterations allowed is reached. This convergence criterion for this analysis is shown in equation B.8

$$\frac{b^{k+1} - b^k}{b^k} \leq 0.001 \quad (\text{B.8})$$

This convergence criteria shown must be met for both perfusion and contact resistance estimates independently. This parameter estimation method uses a whole domain method, meaning the model is run once with a given estimate for perfusion and contact resistance for each Gaussian iteration. Specifically, one set of parameters is estimated for the entire data set. A flowchart of the parameter estimation procedure utilizing the whole domain method is shown in Figure 28.

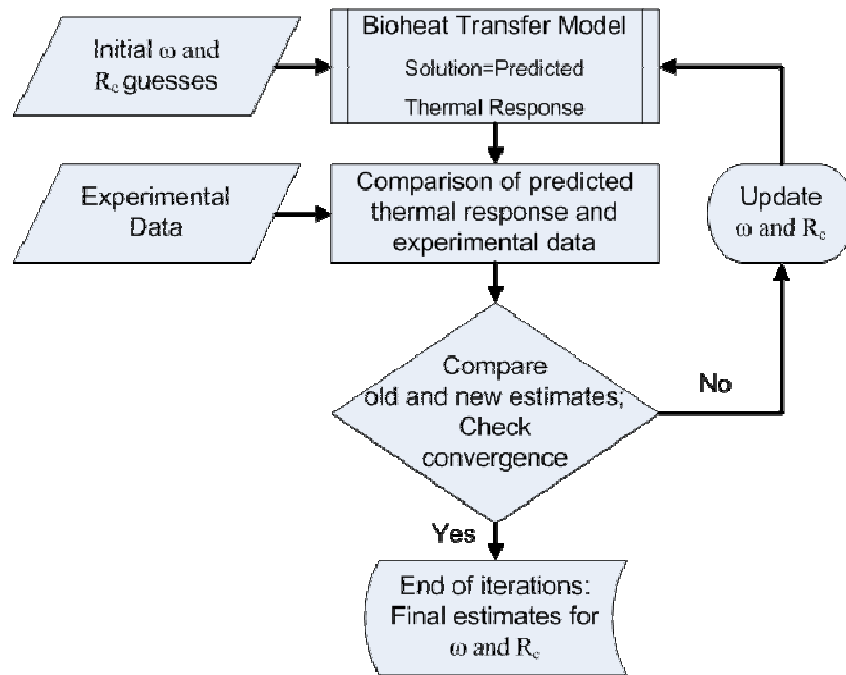


Figure 28. Flowchart of the parameter estimation procedure using the whole domain method.

## Parameter Estimation Code

The parameter estimation routine and how it works with other related programs is shown here.

The flowchart of the developed program is shown in Figure 29.

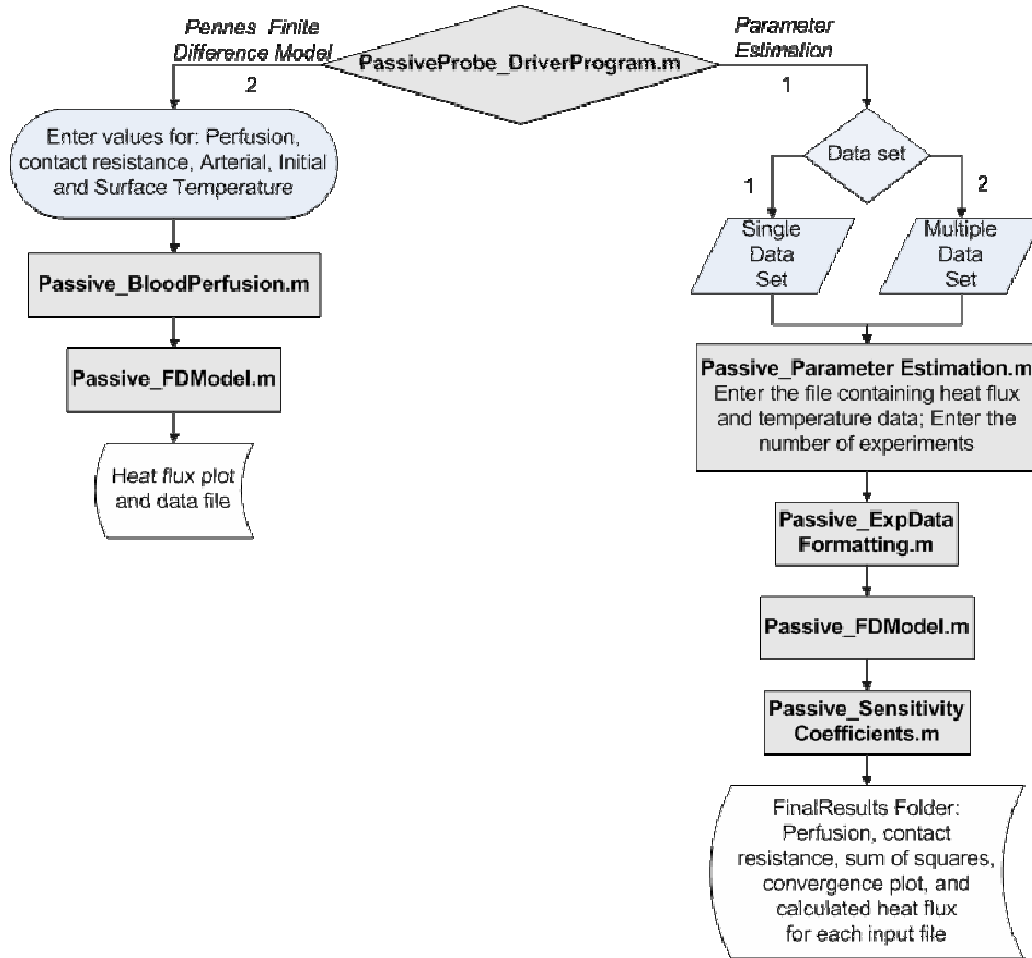


Figure 29. Flowchart of `PassiveProbe_DriverProgram.m` and incorporated Pennes Finite Difference Model and Parameter Estimation programs.

## PassiveProbe\_DriverProgram.m

```
clear all;
close all;
clc;
% This driver program written by Ashvin Mudaliar on 21st of March 2007.
% This code is strictly for passive probe only, the thermal event applied
% to the finite difference model is the temperature measured by pressed
% thermocouple

Run_Choice = input('Enter 1 to run Parameter Estiamtion and 2 Finite Difference Model: ');

if Run_Choice == 2
    Passive_BloodPerfusion;
else
    Input_Choice = input('Enter 1 for one set of data and 2 for multiple set of data: ');
    a = '.txt';

    if Input_Choice == 1
        filenameumber = input('Enter the filename: ');
        d = num2str(filenameumber);
        z = char(d);
        q = [z,a];
        [FinalP2, FinalCR2, FinalSS2] = Passive_ParameterEstimation(q,d);
    else
        filename = input('Enter the text files having heat flux and temperature info: ');
        NumofData = input('Enter the number of Experiments: ');
        char d;
        y1 = load(filename, '%f');

        for count = 1:NumofData
            filenameumber = y1(count,1);
            d = num2str(filenameumber);
            z = char(d);
            q = [z,a];
            [FinalP2, FinalCR2, FinalSS2] = Passive_ParameterEstimation(q,d);
        end
    end
end
```

```

    Perfusion(count) = FinalP2;
    CR(count) = FinalCR2;
    SS(count) = FinalSS2;

end

filepath = 'C:\MATLAB6p5\work\PassiveCode\FinalResults\FinalEstimates';
suffix = '.txt';
fulloutputname = strcat(filepath,suffix);
fid = fopen(fulloutputname,'w');
fprintf(fid,'***Parameter Estimation for All Runs***\n\n');
fprintf(fid,'Perfusion (ml/ml/s) \t Contact Resistance (m^2-K/W) \t Sum of the Squares \n');
fprintf(fid,'-----\t ----- \t -----\n');

for count = 1:NumofData
    fprintf(fid,'%10.5f \t %28.5f \t %26.5f \n', Perfusion(count), CR(count), SS(count));
end
fclose(fid);
end
end

```

## Passive\_ParameterEstimation.m

```
function[FinalP, FinalCr, FinalSS] = Passive_ParameterEstimation(filename1,d)
```

```
% ***** %
```

```
%% PARAMETER ESTIMATION ROUTINE
```

```
%%      by Ashvinikumar Mudaliar dated 21st March 2007
```

```
% ***** %
```

```
global N NP temperatures
```

```
global start stop
```

```
    % starts clock for program run-time
```

```
% ***** Call ExpDataFormatting m-file ***** %
```

```
 %[variables,initial_guesses,temperatures,dataout] = ExpDataFormatting_SP(filename1,filename2);
```

```
 [time,initial_guesses,temperatures,variance,SkinTemp,heat_flux,const5,dt] =
```

```
 Passive_ExpDataFormatting(filename1,d);
```

```
 Y = heat_flux';
```

```
 A = time';
```

```
 NTSTP = const5;
```

```
 %Var = dataout(3,:);
```

```
 Var = variance';
```

```
 MaxIt = 30;
```

```
 BS = initial_guesses;
```

```
 NP = 2;
```

```
 Tarterial = temperatures(1); Ttop = temperatures(2); Tskin_avg = mean(SkinTemp);
```

```
% ***** %
```

```
%% Create text file where output data will be saved
```

```
z='C:\MATLAB6p5\work\PassiveCode\FinalResults\Estimates';
```

```
q=[z,d];
```

```
filepath=q; % ---> Make sure you have the correct
```

```
suffix='.txt'; % directory name for MatLab on
```

```
fulloutputname=strcat(filepath,suffix); % the computer you are using.
```

```

fid=fopen(fulloutputname,'w');
fprintf(fid,'***PARAMETER ESTIMATION ROUTINE*** \n\n');
fprintf(fid,'Input Files: %s, ', filename1); %fprintf(fid,'%s \n', filename2);
fprintf(fid,'Date & Time: %4.0f/%02.0f/%02.0f, %02.0f:%02.0f:%02.0f\n\n', clock);
fprintf(fid,'Tarterial = %4.2f \n',Tarterial);
fprintf(fid,'Ttop = %4.2f \n',Ttop);
fprintf(fid,'Average Skin Temperature = %4.2f \n',Tskin_avg);
% fprintf(fid,'T_BottomThermocouple = %4.2f \n',Tinit1);
% fprintf(fid,'T_Sensor = %4.2f \n\n',Tsensor);
fprintf(fid,'Starting Line #: %5.0f \n', start);
fprintf(fid,'Ending Line #: %5.0f \n\n', stop);
fprintf(fid,' Perfusion (mL/mL/s) \t Contact Resistance (m^2-K/W) \t Sum of Squares\n');
fprintf(fid,'----- \t ----- \t ----- \n');

% *****
% ***** Start of Sequential Gauss Estimation Scheme ***** %

ConvTest = 0;
control =1;

while control < MaxIt

    if ConvTest == 0

% ***** Call MODEL m-file ***** %
        [TIME, SMOOTHPQ] = Passive_FDMModel(BS, temperatures, NTSTP, SkinTemp, dt);
% ***** %
        Qpredicted = SMOOTHPQ;    % save for plotting on final iteration

% ***** Call SENSITIVITY COEFFICIENTS m-file ***** %
        SC = Passive_SensitivityCoefficients(BS,temperatures, SMOOTHPQ, NTSTP, SkinTemp, dt);
% ***** %

%% ----- Calculate the sum of squares (SSy)

```

```

Resid = (Y - SMOOTHPO);
SSy = sum(Resid.^2./Var);
%   RSSy = sum(RS.^2);
%
%% ----- Calculate the "C" matrix
for k = 1:NP
    for k1 = 1: NP
        C(k1,k) = sum(SC(:,k).*SC(:,k1)./Var);
    end
end

%% ----- Calculate "D"
for k = 1:NP
    D(k) = sum(SC(:,k).*Resid./Var);
end

%% ----- Calculate the "P" matrix from the "C" matrix coefficients
PINV = C;

if NP == 1
    P(1,1) = 1./PINV;
else
    P = inv(PINV);    % invert C matrix
end

DeltaB = [0 0];
for k = 1:NP
    for j = 1:NP
        DeltaB(k) = DeltaB(k) + (P(j,k)*D(j));
    end
end

for k = 1:NP
    B(k) = BS(k) + DeltaB(k)/2;
end

%   if B(1) <= 0

```

```

%      B(1) = 0.000001;
%      end
      if B(2)<=0
          B(2) = 0.000001;
      end

      for k = 1:NP
          CI(k) = sqrt(abs(P(k,k)))*1.96;    % 95% confidence interval
      end

% ***** End of Sequential Gauss Estimation Scheme ***** %
% ***** %

%% Check the parameter estimates for w and Rc against the criteria for a
%% converged solution (ratio <= 0.0001). Update "change" accordingly.

      change = 0;

      for j = 1:NP
          Ratio = abs((B(j) - BS(j))./BS(j));
          if Ratio <= 0.0001
              change = change +1;
          end
      end

%% Check to see that both paramters have converged. If not, check to see if
%% the maximum number of iterations have been used. If not, then program
%% runs through Gaussian estimation loop again using the updated
%% parameter estimates as the initial guesses.

      outputs(1,control) = B(1);
      outputs(2,control) = B(2);
      outputs(3,control) = SSy;
      outputs';

      if change == NP
          control = MaxIt + 1;

```

```

fprintf(fid,'%10.5f %28.5f %26.5f \n\n',outputs);
fprintf(fid,'Final Perfusion Estimate (mL/mL/s) = %6.5f \n', B(1));
fprintf(fid,'Final Contact Resistance Estimate (m^2-K/W) = %6.5f \n', B(2));
fprintf(fid,'Sum of Squares for Final Estimates = %6.5f \n', SSy);
%   fprintf(fid,'Sum of Residual Squares for Final Estimates = %6.5f \n', RSSy);
fclose(fid);
figure(1)
plot(time,Y, time,Qpredicted,'--r');
xlabel('Time (sec)'); ylabel('Heat Flux (W/m^2)')
legend('Experimental','Predicted')
title('Heat flux data for the Flow = cc/min');
grid on;
else
    BS = B;
    control = control+1;
end

if control == MaxIt
    fprintf(fid,'%13.5f %28.5f %26.5f \n\n',outputs);
    fprintf('Maximum number of iterations reached. ');
    fclose(fid);
end

end % end "if" statement
end % end "while" statement

FinalP=B(1);
FinalCr=B(2);
FinalSS=SSy;
%open Estimates.txt
h=figure(1);
z='C:\MATLAB6p5\work\PassiveCode\FinalResults\Fig';
q=[z,d];
filepath=q;
suffix='.fig';
fullout=strcat(filepath,suffix);

```

```

saveas(h,fullout);
% _____
% % Writing Predicted heat flux data
for i = 1:const5
    ModelOutputs(1,i) = A(i);
    ModelOutputs(2,i) = SMOOTHPQ(i);
end
z ='C:\MATLAB6p5\work\PassiveCode\FinalResults\HF'; % Make sure you have the correct
q=[z,d];
filepath = q; % ---> Make sure you have the correct
suffix='.txt'; % directory name for MatLab on
fulloutput=strcat(filepath,suffix); % the computer you are using.
fid=fopen(fulloutput,'w');
fprintf(fid,'***Predicted Heat Flux (W/m^2)*** \n\n');
fprintf(fid,'Date & Time: %4.0f/%02.0f/%02.0f, %02.0f:%02.0f:%02.0f\n\n', clock);
fprintf(fid,'Tarterial = %4.2f \n',temperatures(1));
fprintf(fid,'Ttop = %4.2f \n',temperatures(2));
fprintf(fid,'T_initial = %4.2f \n\n',Tskin_avg);
fprintf(fid,' Time (sec) \t\t Heat Flux (W/m^2) \n');
fprintf(fid,'----- \t ----- \n');
fprintf(fid,' %8.5f %20.5f \n', ModelOutputs);
fclose(fid);
% % _____
close all;

% t - total run time for program

```

## Passive\_ExpDataFormatting.m

```
% Ashvin Mudaliar Dated 03/20/2007
% Data formatting as requested by Patricia Ricketts for passive probe
% testing

function [time,initial_guesses,temperatures,variance,SkinTemp,...
    heat_flux,const5,dt] = Passive_ExpDataFormatting(filename1,d)

format short e;

global N NP
global start stop

y=load(filename1, '%f');
% y=load('303.txt');
[maxv ind1] = max(y(1:end,2));
%starting point of the heat flux data
start= ind1;%input('Enter starting point of thermal event: ');
% ending point from heat flux data
stop= length(y(1:end,2));%input('Enter stopping point of thermal event: ');

time_steps = stop-start+1;
TempTime = y(:,1); %Sampling frequency fixed at 12Hz
dt = TempTime(2)- TempTime(1); %Time Step
time = dt:dt:dt*time_steps; %Creating Time vector during thermal event

% initial guesses for perfusion (1) and contact resistance (2)
initial_guesses(1)=0.0001; %Perfusion
initial_guesses(2)=0.0001; %Contact Resistance

ArtTemp = mean(y(1:start-1,4)); % Arterial Temperature
TopTemp = mean(y(1:start-1,5)); % Top Temperature

PressedTemp = y(:,3); % Experimental Air Temp. , Channel 3 reading from Old DAQ
SkinTemp = PressedTemp(start:stop); %Temperature during the thermal event
temperatures(1) = ArtTemp;% Arterial Temperature.
temperatures(2) = TopTemp; % Top Temperature
```

```

% Removing the zero offset in heat flux measurement from the Amplifier
q = y(:,2); % Heat flux;
offset = mean(q(1:start-1)); %calculating the offset heat flux
const3 = length(q); %length of the Experimental heat flux

for i=1:const3
    Actual_heat_flux(i) = q(i)- offset; %Removing the offset in the measurement
end

% figure(2)
% plot(y(:,1),Actual_heat_flux);
% xlabel('Time (s)');
% ylabel('Heat flux (W/m^2)');
% title('Raw heat flux data');

heat_flux = Actual_heat_flux(start:stop); % Thermal event heat flux
const5 = length(heat_flux);

% option for plotting pressed thermocouple temperature
% figure(3)
% plot(time, SkinTemp);
% xlabel('Time (s)');
% ylabel('Temperature');
% title('Skin temperature during the thermal event');

%Option for plotting the scaled heat flux data during the thermal event for
%big probe
% figure(4)
% plot(time, heat_flux, 'r--');
% xlabel('Time (s)');
% ylabel('Heat flux (W/m^2)');
% title('Heat flux during the thermal event');

% Variance for the heat flux data
Var1 = var(heat_flux);

```

```
% Weighing the residual by factor of 1000. The first 5 seconds of data
% is dominated contact resistance. The region of interest is after 15
% seconds where perfusion is dominant
for i = 1:const5
    if i <= 60
        variance(i) = Var1*1000;
    else
        variance(i) = Var1;
    end
end

%*****End of Formatting Experimental Data*****
```

## Passive\_FDModel.m

```
function [TIME, SMOOTHQ] = Passive_FDModel(BS, temperatures,NTSTP,SkinTemp,dt)
% clc;
% clear all;
%Domain details for sensor and tissue
Rs = 0.004275;% Radius of sensor
Rt = Rs*2; %Tissue Radius
Tiss_t = 0.0127; %input(' Thickness of the Tissue'); % Sponge thickness

Radial_nodes = 15;% Nodes on sensor surface
Nodes_Rs = Radial_nodes+1; %adding imaginary nodes to sensor
Nodes_Rt = 2*Radial_nodes+2; %nodes on tissue
Nodes_Zt = 51*5-1;%*Nodes_Zs; % number of nodes along thickness of the tissue

dr = Rs/(Radial_nodes); %spacing between the nodes in radial direction
r = dr/2:dr:Rt-dr/2; % Radius discretized
dz = (Tiss_t)/(Nodes_Zt); % Node spacing in axial direction
z = dz/2:dz:Tiss_t-dz/2; % Thickness discretized

% Properties of the Tissue
rho_t = 998.2; %density of tissue in kg/m^3
sp_heat_t = 4182; %Specific heat of tissue J-kg/K
k_t = 0.5723;% Thermal conductivity of tissue W/m-K
alpha_t = k_t/(rho_t*sp_heat_t); %Thermal diffusivity of the tissue

%Initial Temperature and other required data
Tart = temperatures(1); %Arterial Temperature
Tskin = SkinTemp; %temperatures(3); %Skin Temperature
TopT = temperatures(2); % Top Thermocouple

%Time step for 2D Finite Difference Model
dt1 = dt;%FD_tstp;%FD_tstp; %time step sec
Ta = Tart; % Just allotting Ta as Arterial Temperature
w = BS(1); %blood perfusion in ml/ml/s
Rc = BS(2); %Contact resistance m^2-K
```

```

%
% Initial condition/temperature for tissue
T(1,1:Nodes_Rt) = TopT;
T(Nodes_Zt,1:Nodes_Rt) = Tart;
for i = 2:Nodes_Zt-1
    T(i,1:Nodes_Rt) = T(i-1,1:Nodes_Rt)+ (T(Nodes_Zt,1:Nodes_Rt)-T(1,1:Nodes_Rt))/(Nodes_Zt-1);
end

%
%Defining constants for Tissue
A1t = -alpha_t*dt1/(2*dz^2);
B1t = 1 + (alpha_t*dt1/dz^2) + w*dt1/2;
B2t = 1 + (alpha_t*dt1/dr^2) + w*dt1/2;
D1t = 1 - (alpha_t*dt1/dr^2) ;
D2t = 1 - (alpha_t*dt1/dz^2) ;
for j = 2:Nodes_Rt-1
    C1t(j-1) = (alpha_t*dt1/(2*dr))*(1/dr-1/(2*r(j-1)));
    E1t(j-1) = (alpha_t*dt1/(2*dr))*(1/dr+1/(2*r(j-1)));
end
%
% Matrix elements for Axial sweep in Tissue

C1 = k_t/dz; % constant 1 from FD conduction coefficient
C2 = (dz/(2*k_t) + Rc); % constant 2 from FD at the interface of sensor and tissue
C3 = rho_t*sp_heat_t*w*dz; % constant 3 from FD in axial conduction
% C4 = rho_t*sp_heat_t*w*dr; % constant 4 from FD in radial conduction

for j = 2:Nodes_Rs
    A(1,j) = 0;
    B(1,j) = 1 + C1*C2+ C2*C3;
    C(1,j) = -C1*C2;

    A(Nodes_Zt,j) = -1;
    B(Nodes_Zt,j) = 1;
    C(Nodes_Zt,j) = 0;
end

```

```

for j = Nodes_Rs+1:Nodes_Rt-1
    A(1,j) = 0;
    B(1,j) = C1 + C3;
    C(1,j) = -C1;

    A(Nodes_Zt,j) = -1;
    B(Nodes_Zt,j) = 1;
    C(Nodes_Zt,j) = 0;
end

for i = 2:Nodes_Zt-1
    for j = 2:Nodes_Rt-1
        A(i,j) = A1t;
        B(i,j) = B1t;
        C(i,j) = A1t;
    end
end

% _____
% Matrix elements for Radial sweep in Tissue
for i = 1: Nodes_Zt
    D(i,1) = 0;
    E(i,1) = 1;
    F(i,1) = -1;

    D(i,Nodes_Rt) = -1;
    E(i,Nodes_Rt) = 1;
    F(i,Nodes_Rt) = 0;
end

for i = 1: Nodes_Zt
    for j = 2:Nodes_Rt-1
        D(i,j) = -C1t(j-1);
        E(i,j) = B2t;
        F(i,j) = -E1t(j-1);
    end
end

```

```

%_____

for t = 1:NTSTP %time counter

%_____Axial Sweep for Tissue_____
%Top & Bottom boundary condition
    for j = 2:Nodes_Rs
        RHT1(1,j) = Tskin(t);
        RHT1(Nodes_Zt,j) = 0;
    end

    for j = Nodes_Rs+1:Nodes_Rt-1
        RHT1(1,j) = C3*Ta;
        RHT1(Nodes_Zt,j) = 0;
    end

%Top & Bottom boundary condition

%Middle Columns of the Tissue
    for i = 2:Nodes_Zt-1
        for j = 2:Nodes_Rt-1
            RHT1(i,j) = C1t(j-1)*T(i,j-1) + D1t*T(i,j) + E1t(j-1)*T(i,j+1)+ Ta*w*dt/2;
        end
    end

%Middle Columns of the Tissue

%Thomas Algorithm starts
for j = 2:Nodes_Rt-1
    PT1(1,j) = B(1,j);
    QT1(1,j) = RHT1(1,j)/PT1(1,j);

    for i = 2:Nodes_Zt
        PT1(i,j) = B(i,j)-A(i,j)*C(i-1,j)/PT1(i-1,j);
    end
end

```

```

    QT1(i,j) = (RHT1(i,j)-A(i,j)*QT1(i-1,j))/PT1(i,j);
end
T(Nodes_Zt,j) = QT1(Nodes_Zt,j);

%Backward substitution

for k =Nodes_Zt-1:-1:1
    T(k,j) = QT1(k,j) - C(k,j)*T(k+1,j)/PT1(k,j);
end
end
% Thomas Algorithm ends

%Temperature updated to satisfy boundary condition
T(1:Nodes_Zt,1) = T(1:Nodes_Zt,2);
T(1:Nodes_Zt,Nodes_Rt) = T(1:Nodes_Zt,Nodes_Rt-1);
%_____Axial Sweep for Tissue ends_____

%_____Radial Sweep of Tissue begins_____

%LHS & RHS boundary condition

for i = 1:Nodes_Zt
    RHT2(i,1) = 0;
    RHT2(i,Nodes_Rt) = 0;
end

%LHS & RHS boundary condition

%Middle Columns of the Tissue
for j = 2:Nodes_Rt-1
    for i = 2:Nodes_Zt-1
        RHT2(i,j) = -A1t*T(i-1,j) + D2t*T(i,j) -A1t*T(i+1,j)+ Ta*w*dt/2;
    end
end

%Middle Columns of the Tissue

```

```
%Thomas Algorithm starts for the region below the sensor
```

```
for i = 2:Nodes_Zt-1
```

```
    PT2(i,1) = E(i,1);
```

```
    QT2(i,1) = RHT2(i,1)/PT2(i,1);
```

```
    for j = 2:Nodes_Rt
```

```
        PT2(i,j) = E(i,j)-D(i,j)*F(i,j-1)/PT2(i,j-1);
```

```
        QT2(i,j) = (RHT2(i,j)-D(i,j)*QT2(i,j-1))/PT2(i,j);
```

```
    end
```

```
    T(i,Nodes_Rt) = QT2(i,Nodes_Rt);
```

```
    %Backward substitution
```

```
    for k = Nodes_Rt-1:-1:1
```

```
        T(i,k) = QT2(i,k) - F(i,k)*T(i,k+1)/PT2(i,k);
```

```
    end
```

```
end
```

```
%Thomas Algorithm ends for the region below the sensor
```

```
%
```

---

```
r1 = r(1:Nodes_Rs-1);
```

```
for i = 2:Nodes_Rs
```

```
    q(i-1) = k_t/(z(2)-z(1))*(T(3,i)- T(2,i));
```

```
    Top1T(i-1) = T(1,i-1); % for calculating resistive heat flux
```

```
    TopT(i-1) = T(2,i-1);
```

```
    BotT(i-1) = T(3,i-1);
```

```
end
```

```
qcond(t) = sum(q*r1')/sum(r1);
```

```
Top(t) = sum(TopT*r1')/sum(r1);
```

```
Bot(t) = sum(BotT*r1')/sum(r1);
```

```
Top1(t) = sum(Top1T*r1')/sum(r1);
```

```
qres(t) = (Top1(t)-Tskin(t))/C2;
```

```
MP = qres';  
vectlength = length(MP);  
SMOOTHQ = MP(1:1:end);  
length(SMOOTHQ);  
TIME(t) = t*dt1;
```

```
end
```

```
% plot(TIME,qres,'-r');
```

## Passive\_SensitivityCoefficients.m

```
function SC = Passive_SensitivityCoefficients(BS, temperatures, SMOOTHPQ,NTSTP,SkinTemp, dt)
```

```
% ***** %
```

```
%% SENSITIVITY COEFFICIENTS
```

```
%% by Ashvin Mudaliar
```

```
% ***** %
```

```
global N
```

```
Beta1 = BS(1);
```

```
Beta2 = BS(2);
```

```
Factor = 1.01;
```

```
Beta1P = Beta1*Factor;
```

```
Beta2P = Beta2*Factor;
```

```
[TIME, SMOOTHPQ1] = Passive_FDModel([Beta1P,Beta2], temperatures, NTSTP,SkinTemp, dt);
```

```
[TIME, SMOOTHPQ2] = Passive_FDModel([Beta1,Beta2P], temperatures, NTSTP,SkinTemp, dt);
```

```
SC(:,1) = (SMOOTHPQ1 - SMOOTHPQ)./(Beta1P - Beta1);
```

```
SC(:,2) = (SMOOTHPQ2 - SMOOTHPQ)./(Beta2P - Beta2);
```

## Passive\_BloodPerfusion.m

```
function Passive_BloodPerfusion
format long e;
% ***** %
%% Formatting for Finite Difference Model
%% by Ashvinikumar Mudaliar march 21st 2007
% ***** %

BS(1) = input('Enter value for blood perfusion (ml/ml/s): ');
BS(2) = input('Enter value for contact resistance (m^2-K/W): ');
temperatures(1) = input('Enter Arterial temperature (C): ');
temperatures(2) = input('Enter Top temperatures (C): ');
PressedTemp = input('Enter Skin temperature (Pressed Thermocouple) (C): ');

dt = 0.08333;
NTSTP = 720;
SkinTemp = PressedTemp*ones(1,NTSTP);
[TIME, SMOOTHQ] = Passive_FDModel(BS, temperatures,NTSTP,SkinTemp,dt);
for i = 1:length(TIME)
    ModelOutputs(1,i) = TIME(i);
    ModelOutputs(2,i) = SMOOTHQ(i);
end
filepath='C:\MATLAB6p5\work\PassiveCode\ModelResults'; % Make sure you have the correct
suffix='.txt'; % directory name for MatLab on
fulloutputname=strcat(filepath,suffix); % the computer you are using.

fid=fopen(fulloutputname,'w');
fprintf(fid,'***TISSUE BIOHEAT TRANSFER MODEL*** \n\n');
fprintf(fid,'Date & Time: %4.0f/%02.0f/%02.0f, %02.0f:%02.0f:%02.0f\n\n', clock);
fprintf(fid,'Arterial Temperature (deg C) = %4.2f \n',temperatures(1));
fprintf(fid,'Top Temperature (deg C) = %4.2f \n',temperatures(2));
fprintf(fid,'Skin Temperature (deg C) = %4.2f \n\n',PressedTemp);
fprintf(fid,'Blood Perfusiuon (ml/ml/s) = %4.2f \n\n',BS(1));
fprintf(fid,'Contact Resistance (m^2-K/W) = %4.2f \n\n',BS(2));
fprintf(fid,' Time (sec) \t\t Heat Flux (W/m^2) \n');
fprintf(fid,'----- \t ----- \n');
fprintf(fid,' %8.5f %20.5f \n', ModelOutputs);
fclose(fid);
```

```
open ModelResults.txt
```

```
figure(1)
```

```
plot(TIME, SMOOTHQ);
```

```
xlabel('Time (sec)'); ylabel ('Heat Flux (W/m^2)');
```

```
title('Heat flux data for the Finite Difference Model');
```

## Appendix C: LabVIEW VI

As discussed previously, LabVIEW 8.2 was used to record all of the experimental data for both the phantom tissue and animal model tests. A LabVIEW Virtual Instrument (VI) was developed to record the heat flux and temperature measurements. Since temperature measurements were made using both thermocouples and thermistors, the VI also provided the necessary voltage for the thermistor measurement circuit. Also, the VI's Block Diagram was programmed to convert each voltage measurement into its corresponding heat flux or temperature value. The heat flux voltage was converted to heat flux ( $\text{W}/\text{m}^2$ ) by multiplying by the sensor's sensitivity provided by Vatel<sup>®</sup>. The thermocouple voltage measurements were converted by multiplying by the thermocouple's sensitivity and then adding the reference temperature. Finally, the VI provided the input voltage for the thermistor circuit and also converted the thermistor voltage measurements to temperature using a polynomial equation derived from the thermistor datasheet. Inputs on the VI's front panel include test length (seconds), reference temperature ( $^{\circ}\text{C}$ ) and heat flux multiplier ( $\text{W}/\text{m}^2\text{-V}$ ).

The Front Panel during testing is shown in Figure 30. As can be seen from the figure, the heat flux is displayed first, followed by the three thermocouple measurements (Pressed, Arterial, and Top), and finally the three thermistor measurements (Block, Arterial, Top). These graphs are updated continuously during each test and allow the user to assess the test run's success immediately.

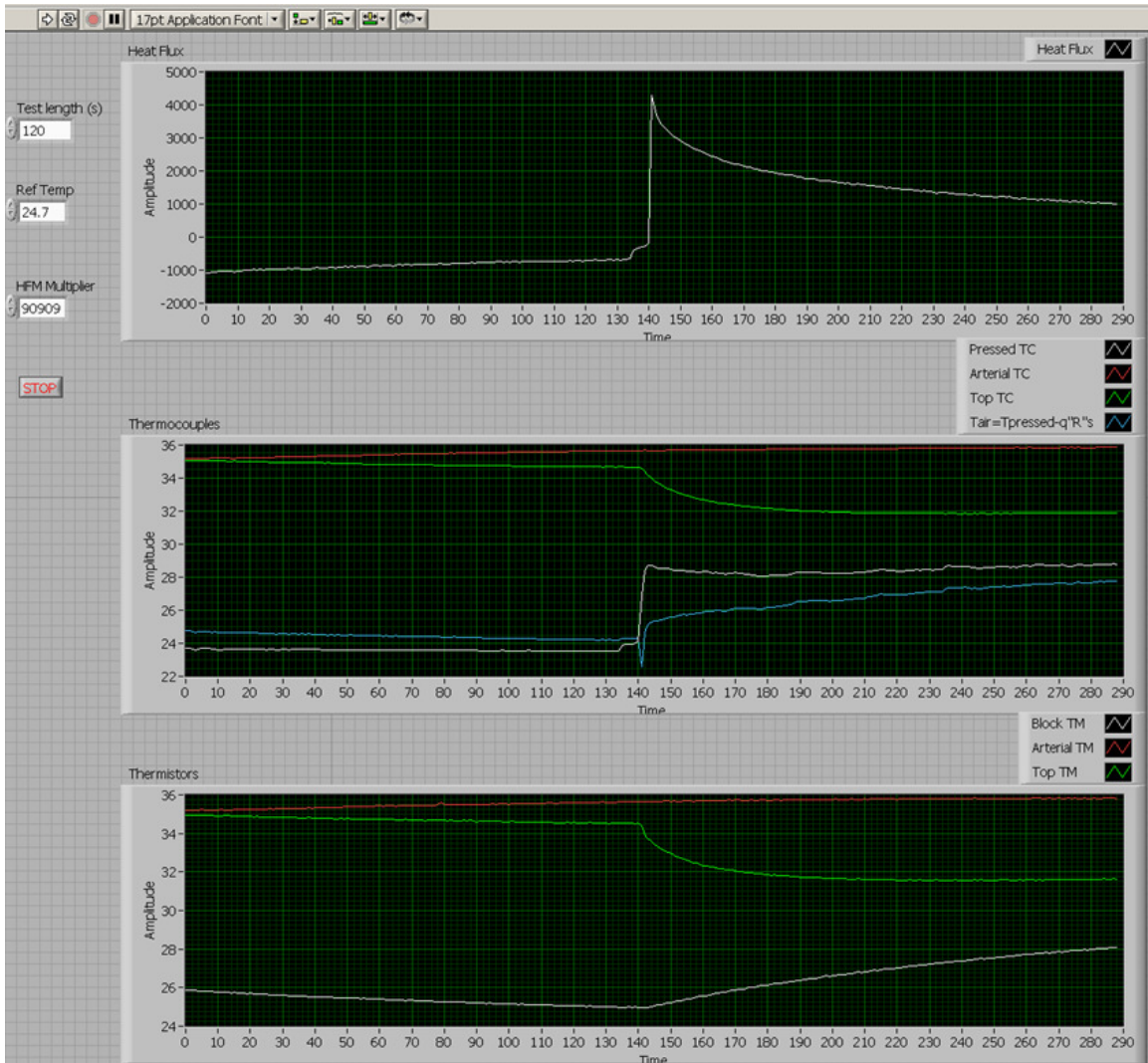


**Figure 30. LabVIEW VI Front Panel used to record all experimental data.**

The LabVIEW Block Diagram is shown in Figure 31. This Block Diagram is a pictorial programming tool used in LabVIEW. The base of this diagram is the **DAQ Assistant2**, which coordinates the recording of the voltage signals. These signals are then converted to their respective measurements as mentioned previously. Next, the converted values are displayed on the graphs located on the Front Panel and shown in Figure 30 using a series of arrays shown in orange. Finally, both the converted and original voltage measurements are recorded to a specified measurement file using the **Write To Measurement File** block. The **Simulate Signal** block is used to provide the input voltage for the thermistor circuit of 1.25V. The **DAQ Assistant** block coordinates this output voltage with the specified channel chosen within the DAQ and connector block.

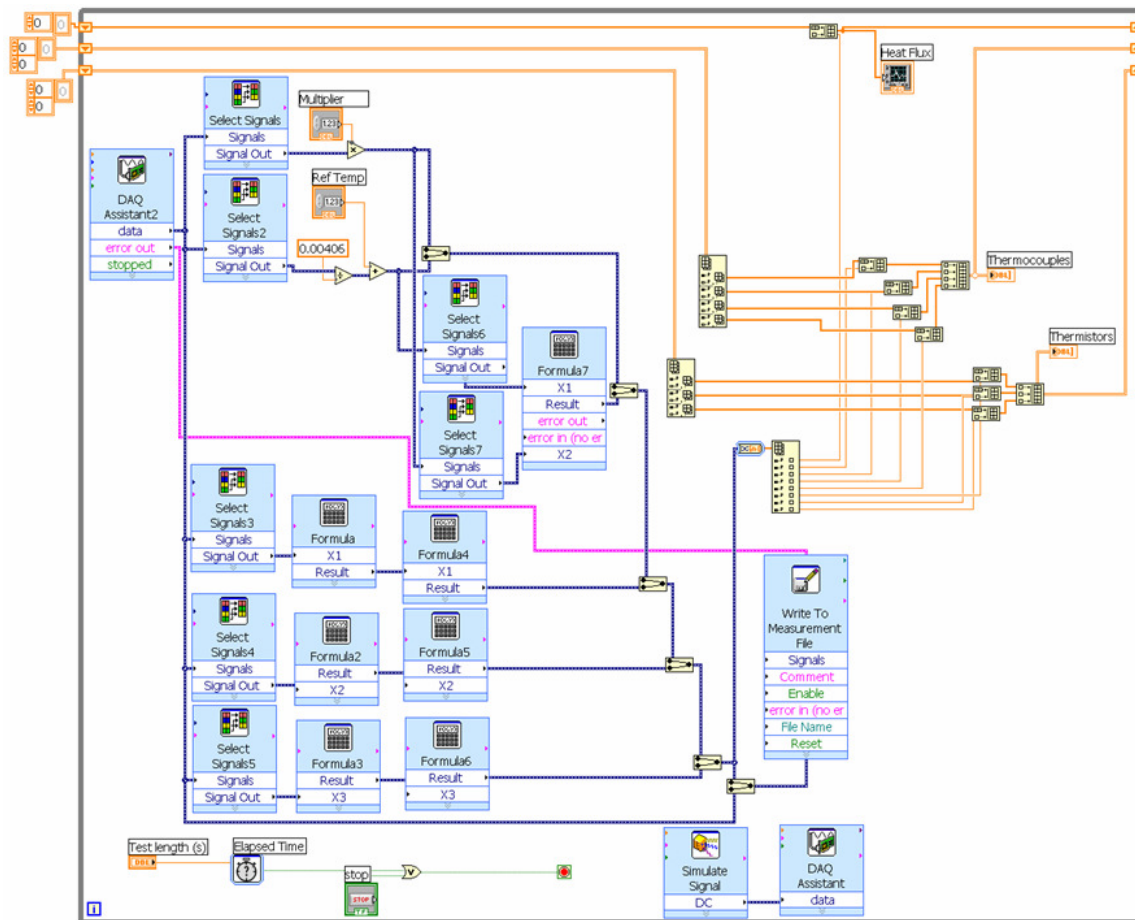


Figure 31. LabVIEW VI Block Diagram used to record all experimental data.

## Appendix D: Experimental Data Analysis

### *Phantom Tissue Model Experimental Data*

The data presented in the paper only included flow rates of 0-20cc/min. The additional results at flow rates of 25 and 30cc/min are shown here. The experimental results for all probes are shown in Figure 32. These experimental results are then compared with the CFD model developed in Fluent in Figure 33.

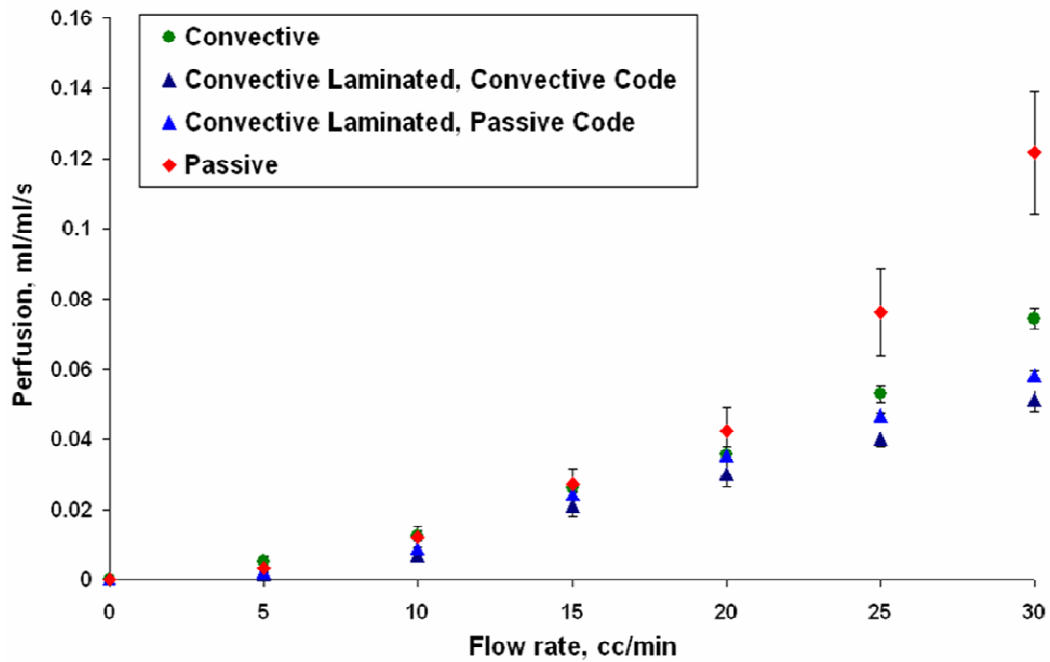


Figure 32. Experimental perfusion results with 95% confidence intervals of the perfusion probes on the phantom tissue model.

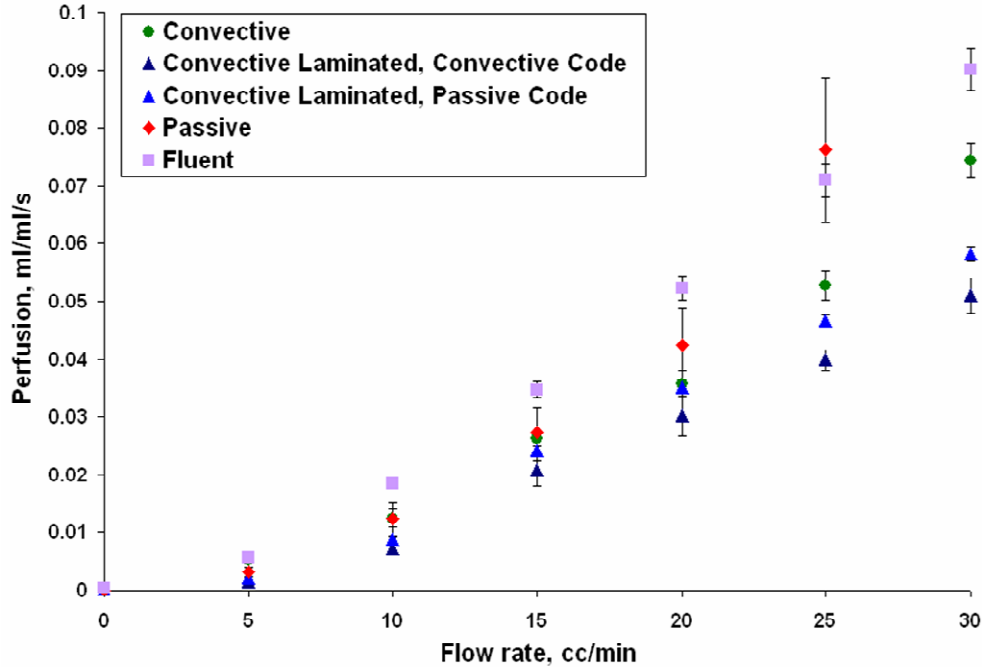


Figure 33. Experimental and Fluent CFD perfusion results with 95% confidence intervals for the phantom tissue model tests.

### Statistical Analysis Summary

This section summarizes the statistical analysis performed on the phantom tissue and exposed rat liver models. First, an overall summary for the model is given. Next, individual summaries are given for each perfusion probe. These summaries include the box plots and tab data obtained from the one-way analysis of variance for each probe as well as the multi-comparison plot to determine whether the means are statistically different from one another.

### Phantom Tissue Model

Table 7. Statistical analysis summary for the phantom tissue model.

Probe	P Value	% Probability Means Are Not Equal	Flow rates Which Are Statistically Different (cc/min)
Passive	0	100	25, 30
Convective	0	100	All
Convective Laminated Convective Code	4.6296E-14	100	0-20
Convective Laminated Passive Code	0	100	0-20

**Passive Perfusion Probe**

ANOVATAB =

'Source'	'SS'	'df'	'MS'	'F'	'Prob>F'
'Columns'	[0.1494]	[ 6]	[ 0.0249]	[122.9242]	[ 0]
'Error'	[0.0156]	[77]	[2.0254e-004]	[ ]	[ ]
'Total'	[0.1650]	[83]	[ ]	[ ]	[ ]

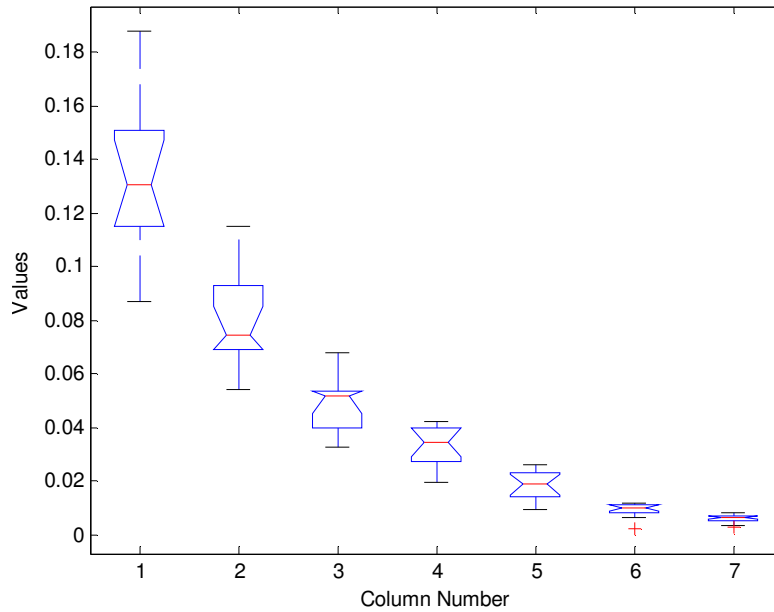


**Figure 34. ANOVA Box plot for the passive perfusion probe on the phantom tissue model.**

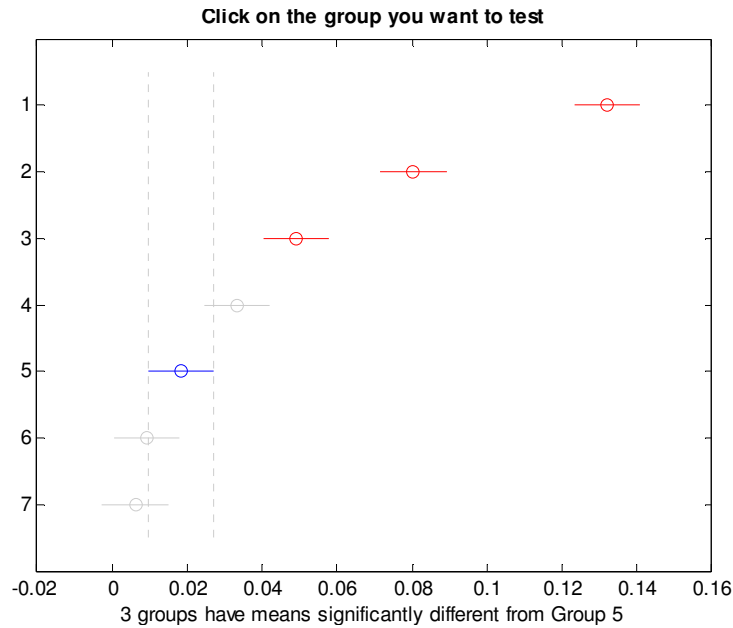


**Figure 35. Multicomparison plot for the passive perfusion probe on the phantom tissue model.**

**Convective Perfusion Probe**

ANOVATAB =

'Source'	'SS'	'df'	'MS'	'F'	'Prob>F'
'Columns'	[0.0566]	[ 6]	[ 0.0094]	[732.3906]	[ 0]
'Error'	[0.0011]	[84]	[1.2883e-005]	[ ]	[ ]
'Total'	[0.0577]	[90]	[ ]	[ ]	[ ]

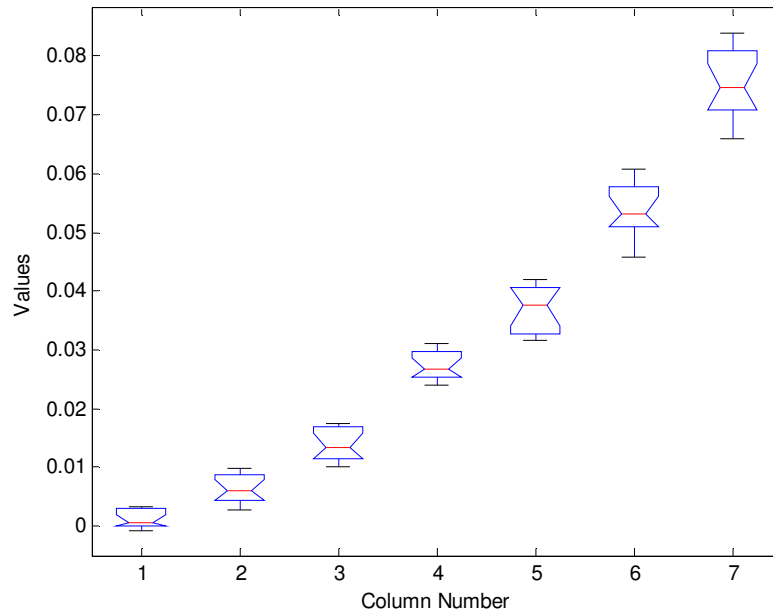


**Figure 36. ANOVA Box plot for the convective perfusion probe on the phantom tissue model**

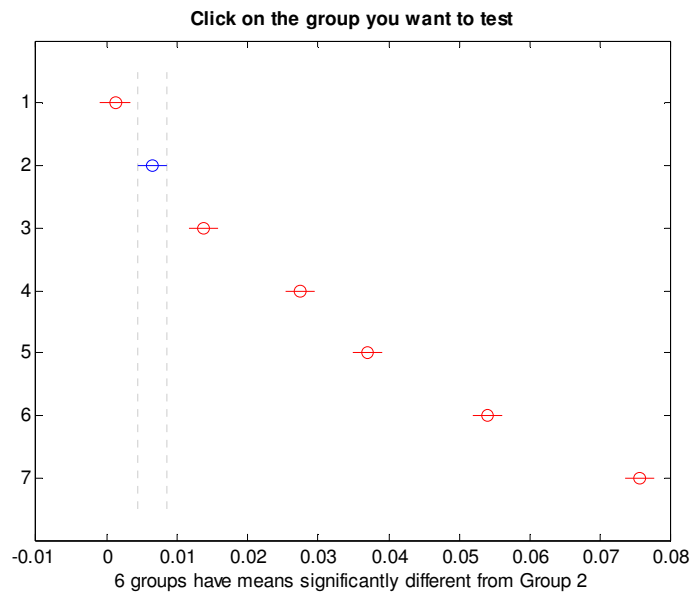


**Figure 37. Multicomparison plot for the convective perfusion probe on the phantom tissue model.**

**Convective Laminated Perfusion Probe – Convective Code**

ANOVATAB =

'Source'	'SS'	'df'	'MS'	'F'	'Prob>F'
'Columns'	[ 0.0071]	[ 6]	[ 0.0012]	[309.8755]	[4.6296e-014]
'Error'	[5.3218e-005]	[14]	[3.8013e-006]	[ ]	[ ]
'Total'	[ 0.0071]	[20]	[ ]	[ ]	[ ]

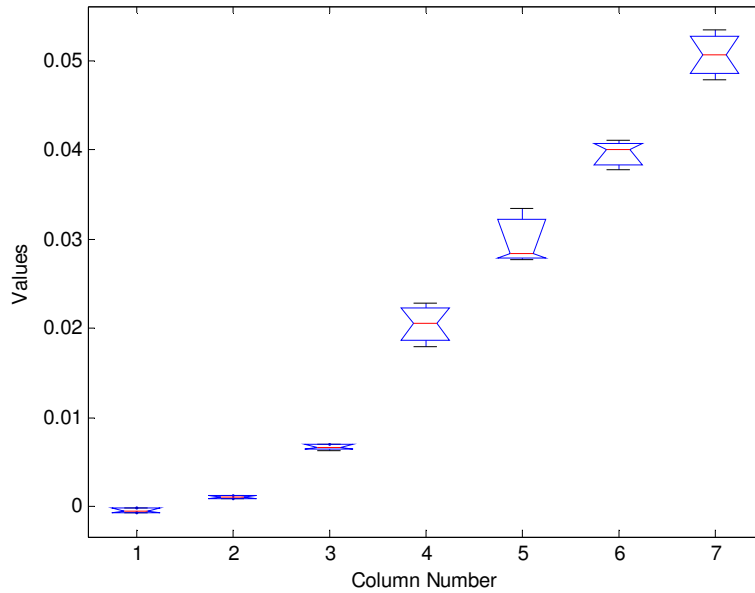


**Figure 38. ANOVA Box plot for the convective laminated perfusion probe with convective code on the phantom tissue model**

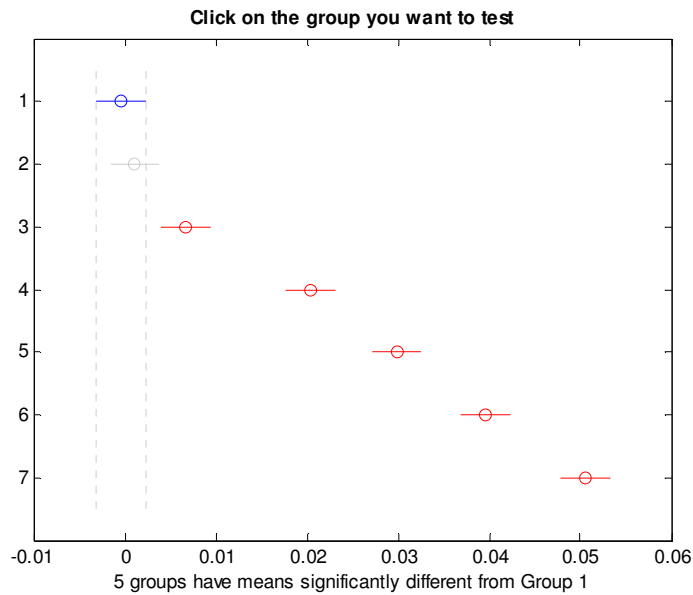


**Figure 39. Multicomparison plot for the convective laminated perfusion probe with convective code on the phantom tissue model.**

**Convective Laminated Perfusion Probe – Passive Code**

ANOVATAB =

'Source'	'SS'	'df'	'MS'	'F'	'Prob>F'
'Columns'	[ 0.0093]	[ 6]	[ 0.0015]	[2.0292e+003]	[ 0]
'Error'	[1.0638e-005]	[14]	[7.5984e-007]	[ ]	[ ]
'Total'	[ 0.0093]	[20]	[ ]	[ ]	[ ]

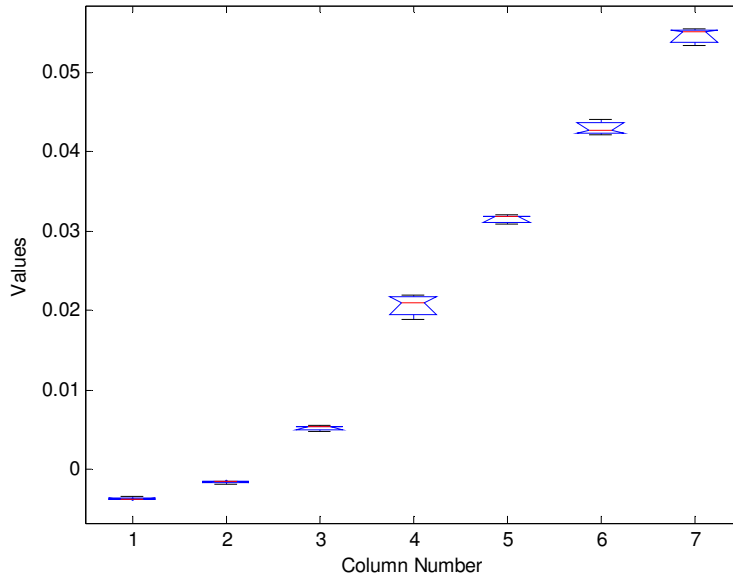


**Figure 40. ANOVA Box plot for the convective laminated perfusion probe with passive code on the phantom tissue model**

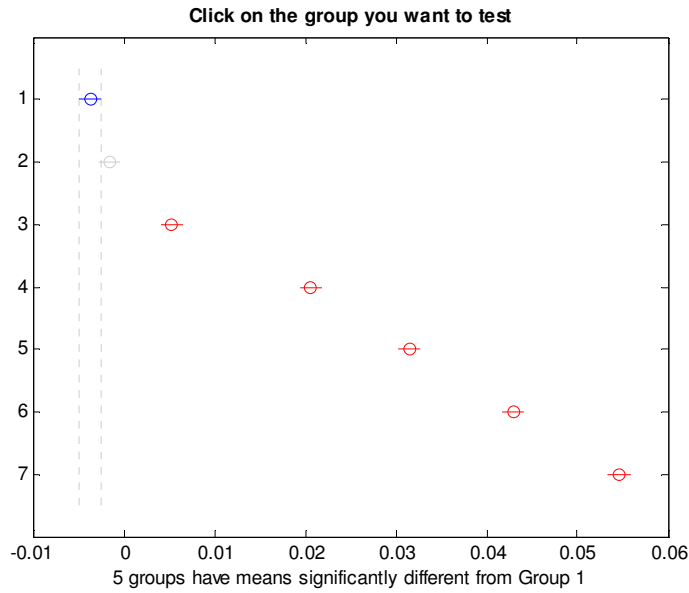


**Figure 41. Multicomparison plot for the convective laminated perfusion probe with passive code on the phantom tissue model.**

## Exposed Rat Liver Model

Table 8. Statistical analysis summary for the exposed rat liver model.

Probe	P Value	% Probability Means Are Not Equal
Passive - Day 1	7.41E-06	100.00
Passive - Day 2	2.84E-05	99.99
Convective	6.79E-05	99.99
Convective Laminated Convective Code	0.0019	99.62
Convective Laminated Passive Code	0.0016	99.68

Note that all cases (initial, occluded and non-occluded) for all probes are statistically different from one another for the exposed rat liver model.

**Passive Perfusion Probe – Day 1**

ANOVA TAB =

'Source'	'SS'	'df'	'MS'	'F'	'Prob>F'
'Columns'	[4.3512e-004]	[ 1]	[4.3512e-004]	[203.5958]	[7.4110e-006]
'Error'	[1.2823e-005]	[ 6]	[2.1372e-006]	[ ]	[ ]
'Total'	[4.4795e-004]	[ 7]	[ ]	[ ]	[ ]

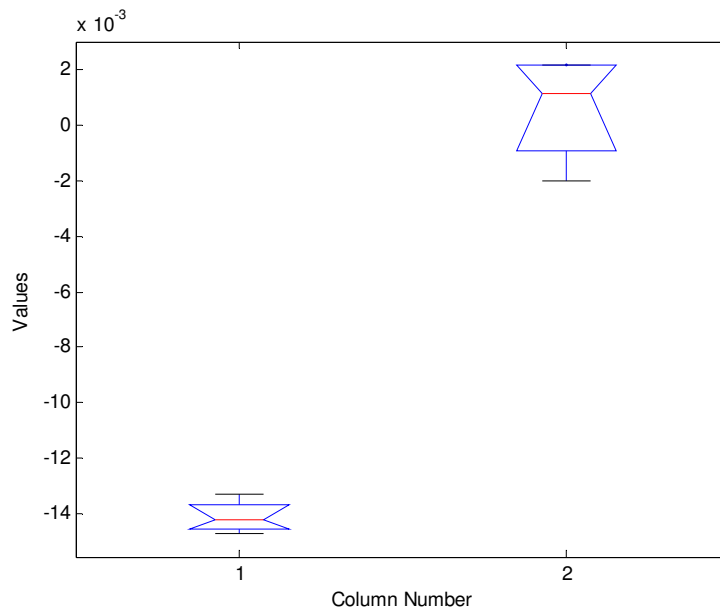


**Figure 42. ANOVA Box plot for the passive perfusion probe (Day 1) on the exposed rat liver model.**

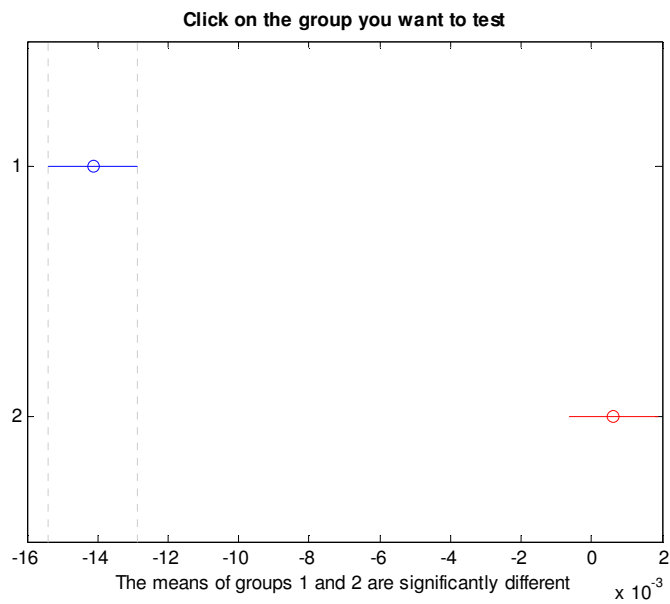


**Figure 43. Multicomparison plot for the passive perfusion probe (Day 1) on the exposed rat liver model.**

**Passive Perfusion Probe – Day 2**

ANOVATAB =

'Source'	'SS'	'df'	'MS'	'F'	'Prob>F'
'Columns'	[6.6121e-004]	[ 1]	[6.6121e-004]	[128.2615]	[2.8370e-005]
'Error'	[3.0931e-005]	[ 6]	[5.1551e-006]	[]	[]
'Total'	[6.9214e-004]	[ 7]	[]	[]	[]

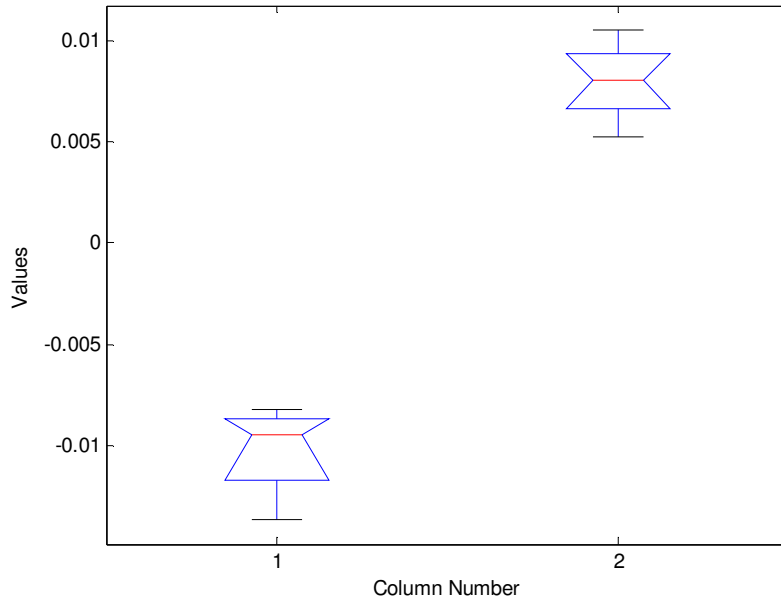


**Figure 44. ANOVA Box plot for the passive perfusion probe (Day 2) on the exposed rat liver model.**

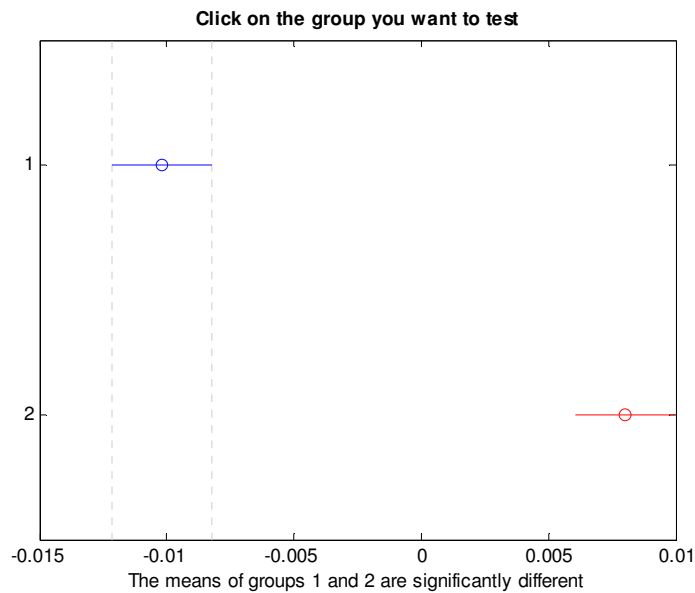


**Figure 45. Multicomparison plot for the passive perfusion probe (Day 2) on the exposed rat liver model.**

**Convective Perfusion Probe**

ANOVATAB =

'Source'	'SS'	'df'	'MS'	'F'	'Prob>F'
'Columns'	[6.2463e-004]	[ 1]	[6.2463e-004]	[94.5588]	[6.7922e-005]
'Error'	[3.9635e-005]	[ 6]	[6.6058e-006]	[ ]	[ ]
'Total'	[6.6427e-004]	[ 7]	[ ]	[ ]	[ ]

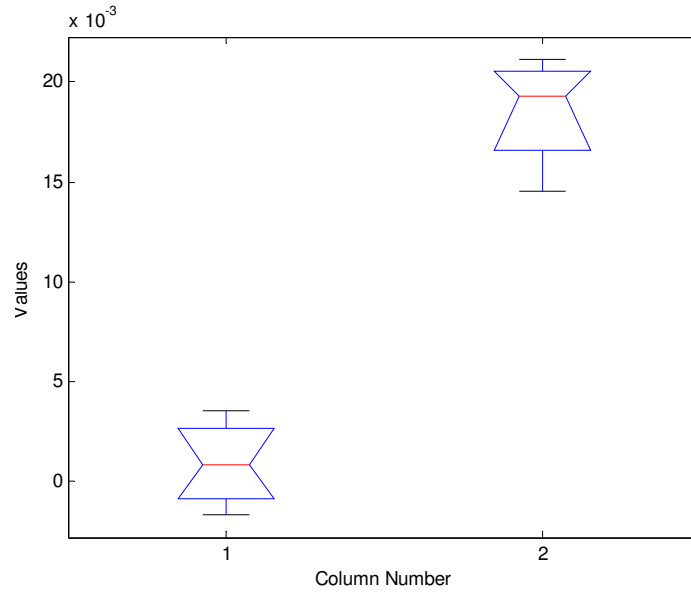


**Figure 46. ANOVA Box plot for the convective perfusion probe on the exposed rat liver model.**

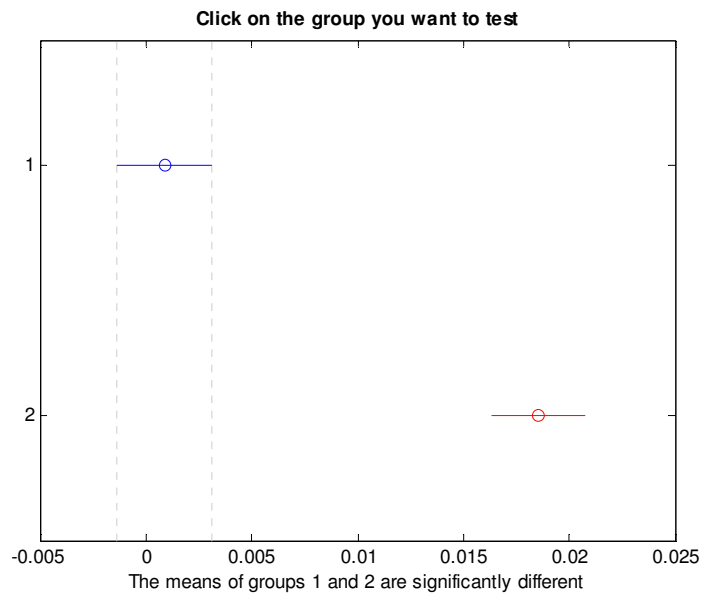


**Figure 47. Multicomparison plot for the convective perfusion probe on the exposed rat liver model.**

**Convective Laminated Perfusion Probe – Convective Code**

ANOVATAB =

'Source'	'SS'	'df'	'MS'	'F'	'Prob>F'
'Columns'	[3.7183e-004]	[ 1]	[3.7183e-004]	[27.5545]	[0.0019]
'Error'	[8.0965e-005]	[ 6]	[1.3494e-005]	[ ]	[ ]
'Total'	[4.5279e-004]	[ 7]	[ ]	[ ]	[ ]

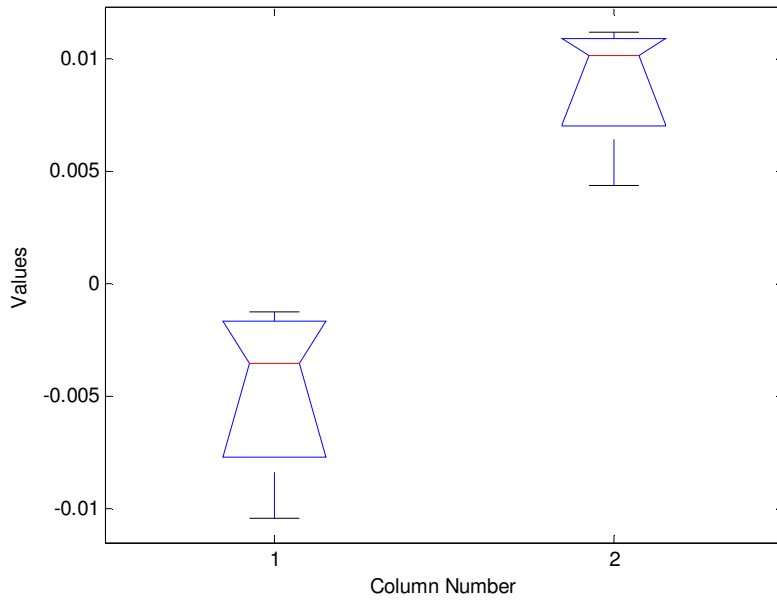


**Figure 48. ANOVA Box plot for the convective laminated perfusion probe with convective code on the exposed rat liver model.**

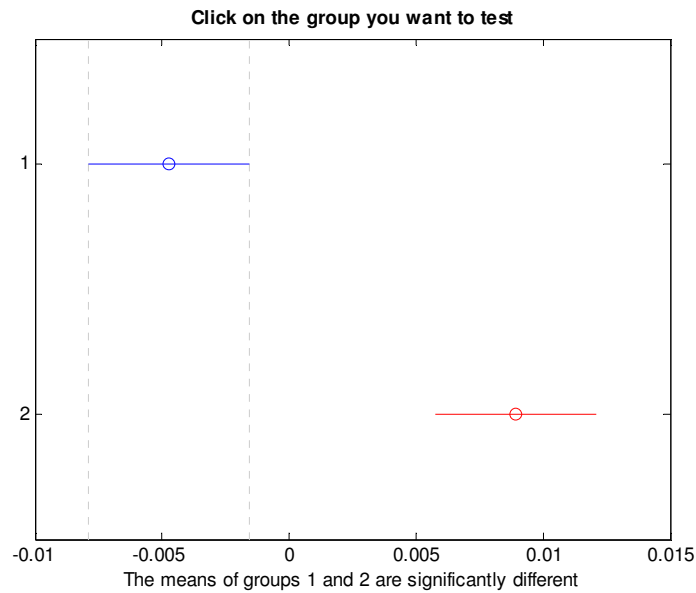


**Figure 49. Multicomparison plot for the convective laminated perfusion probe with convective code on the exposed rat liver model.**

**Convective Laminated Perfusion Probe – Passive Code**

ANOVA TAB =

'Source'	'SS'	'df'	'MS'	'F'	'Prob>F'
'Columns'	[2.9768e-004]	[ 1]	[2.9768e-004]	[29.4797]	[0.0016]
'Error'	[6.0587e-005]	[ 6]	[1.0098e-005]	[]	[]
'Total'	[3.5827e-004]	[ 7]	[]	[]	[]

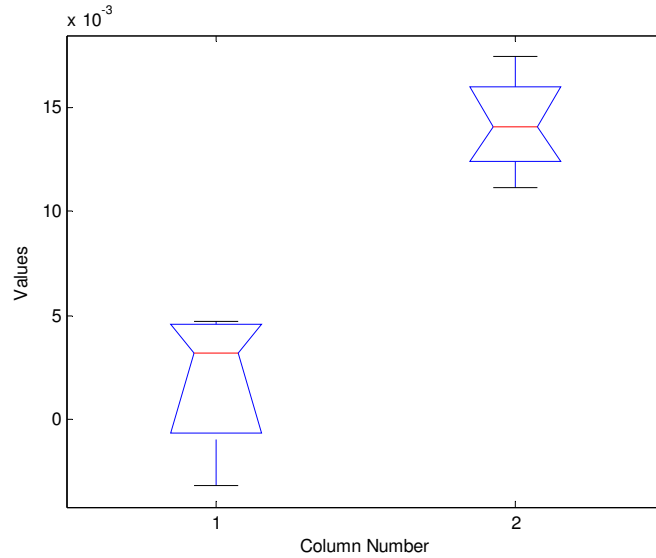


**Figure 50. ANOVA Box plot for the convective laminated perfusion probe with passive code on the exposed rat liver model.**

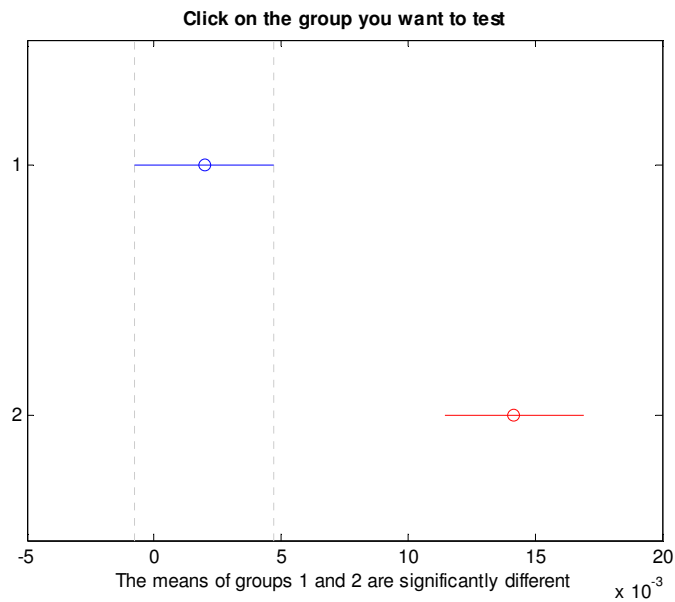


**Figure 51. Multicomparison plot for the convective laminated perfusion probe with passive code on the exposed rat liver model.**

## Appendix E: Data DVD

A DVD disc containing soft copy of thesis, journal paper, all MATLAB codes, Lab view VI's and all the data required to reproduce the results shown here is attached. The DVD is organized as shown:

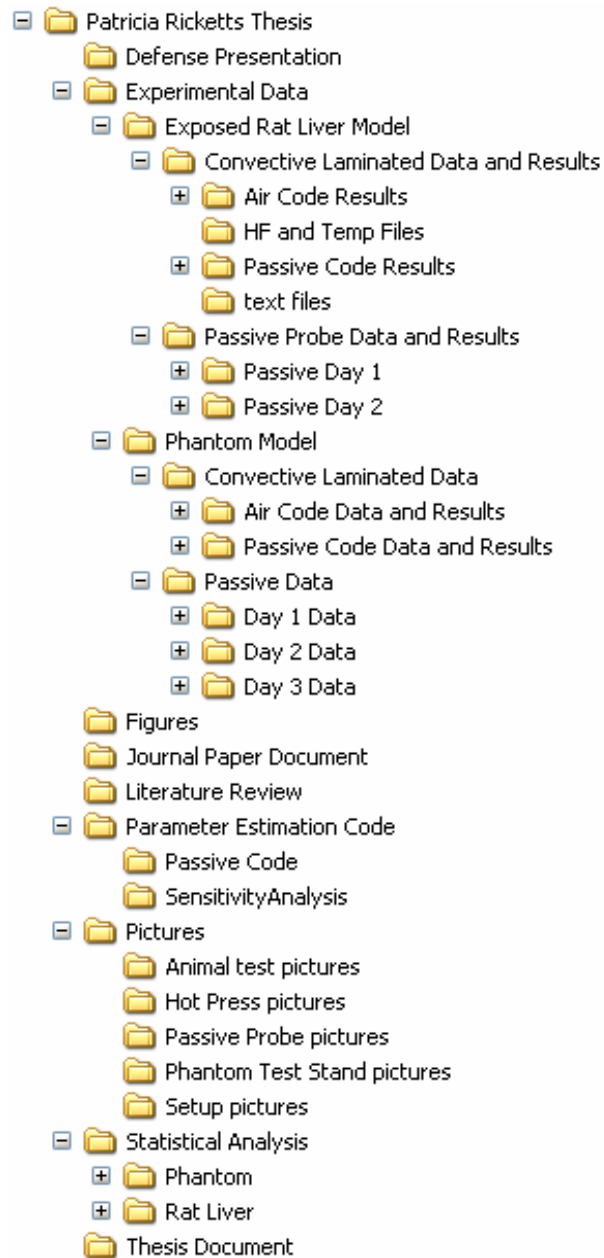


**Figure 52. Organization of attached DVD.**